Wire Grid Polarizer by Angled Deposition Method Using Nanoimprint Lithography

by

Young Jae Shin

A dissertation submitted in partial fulfillment
of the requirements for the degree of
Doctor of Philosophy
(Macromolecular Science and Engineering)
in The University of Michigan
2014

Doctoral Committee:

Professor L. Jay Guo, Chair
Peng-Fei Fu, Dow Corporation
Professor Jinsang Kim
Professor Richard Robertson

© Young Jae Shin

2014

Acknowledgement

Foremost, I would like to express my sincere gratitude to my advisor Prof. L. Jay Guo for the continuous support of my Ph.D. study and research, for his patience, motivation, enthusiasm, and immense knowledge. His guidance helped me in all the time of research and writing of this thesis. I could not have imagined having a better advisor and mentor for my Ph.D. study.

Besides my advisor, I would like to thank the rest of my thesis committee: Prof. Jinsang Kim, Prof. Richard Robertson, and Dr. Peng-fei Fu, for their encouragement, insightful comments, and solving the hard questions.

I thank my fellow lab mates at Guo research Group in University of Michigan: For nanofabrication, Jae Yong Lee, Hyunsoo Kim, Cheng Zhang, Dr. Jong Ok, Dr. Hongseok Youn, Dr. Tao Ling, Dr. Carlos Pina, Dr. Hui Joon Park, Prof. Moon Kyu Kwak Dr. Alex Kaplan, Master. Andrew Hollowell, Prof. Haofei Shi, Ashwin Panday and Chad Huard. For the stimulating discussions, Tae Hee Jang, Taehwa Lee, Sung Yong Seo, Yi-Kuei Wu, and Dr. Masanori Fukuda. Also I thank other group members and my friends in University of Michigan.

Last but not the least, I'd like to present my sincere thankfulness to my dear father and my mother for their great role in my life and their numerous sacrifices for me. Many thanks for my brother for his support and for being truly brother when needed.

Table of Contents

Acknowledgement ii

List of Figures vi

List of Tables x

Abstract xi

Chapter 1 Introduction: background of nanoimprint lithography and polarizer 1

1.1. Motivation of nanoimprint lithography 1
1.2. Nanoimprint lithography 2
1.2.1. Nanoimprint lithography materials 3
1.2.2. Roll to roll nanoimprint lithography. 4
1.3. Motivation of fabricating wire grid polarizer 6
1.3.1. WGP principle 6
1.3.2. Conventional polarizers 7

Chapter 2 Nanoimprinting ultrasmall and high-aspect-ratio structures by using rubber-toughened UV cured epoxy resist 9

2.1. Introduction 9
2.2. Experimental 12
2.2.1. Materials and instruments 12
2.2.2. Nanoimprinting of modulus-tunable UV cure epoxy resist 13
2.2.3. Atomic Layer Deposition (ALD) 13
2.2.4. Reactive ion etching (RIE) 14

2.3. Results and discussion 14
2.3.1. Tuning Physical Property of Resist 14
2.3.2. Nanoimprinting with silicon dioxide mold using the epoxy resins 18
2.3.3. Reducing the trench of the nanopattern 19
2.3.4. Nanoimprinting to get the 20-nm-line-width nanopattern 21
2.3.5. Reactive ion etching (RIE) 23
2.4. Conclusions 26
Chapter 3 Facile route of flexible wire grid polarizer fabrication by angled-depositions of aluminum on two sidewalls of an imprinted nanograting 27
3.1. Introduction 27
3.2. Experimental 29
3.2.1. Materials and synthesis of SSQ 30
3.2.2. Instruments 31
3.2.3. Nanoimprint process 31
3.2.4. Aluminum deposition 32
3.2.5. Plasma Ion etching process 33
3.3. Results and discussion 34
3.3.1. Design consideration of the WGP 34
3.3.2. Synthesis of Epoxy-SSQ and NIL 37
3.3.3. Aluminum deposition and etching 39
3.3.4. Measurement of TM & TE transmission and extinction ratio 40
3.4. Conclusion 42
Chapter 4 Fabrication and Encapsulation of a Short-Period Wire Grid Polarizer with Increased Viewing Angle by the Angled-evaporation Method 43
4.1. Introduction 43
4.2. Experimental 46
4.2.1. Materials and the Synthesis of Imprinting Material 46
4.2.2. Instruments 47
4.2.3. Nanoimprint Process 47
4.2.4. Aluminum Deposition 48

4.2.5. Reactive Ion Etching Process 48
4.2.6. Encapsulation of WGP 48
4.3. Results and Discussion 49
4.3.1. Simulation of Angle Dependency 49
4.3.2. Fabrication of the WGP 51
4.3.3. Optical Properties of the WGP 54
4.3.4. Measurement of the refractive index and thickness of the polymerized epoxy-SSQ . 59
4.3.5. Simulation results for the effect of the coating thickness on TM and TE 61
4.4. Conclusion 63
Chapter 5 Concluding Remarks 64
5.1. Contribution of nanoimprint materials 64
5.2. Contribution of mold fabrication 65
5.3. Contribution of WGP fabrication method 65
5.3.1. Decreasing angular dependency of WGP 66
5.3.2. Encapsulation of WGP 67
Reference 68

List of Figures

Figure 1. 1. A schematic illustration for fabricating nanopatterns by soft nanoimprinting with flexible molds. The left and right columns denote patterning dense dot and hole arrays, respectively, using the molds with opposite sense. Some demolding failures are shown in the left and right bottom panels [35]. 3

Figure 1. 2. (a) Illustration of the overall fabrication procedure of the metal-insulator-metal (MIM)-based nanostructure. The epoxysilsesquioxane (SSQ) pattern was continuously created on the metal-insulator-metal (MIM)-deposited PET substrate by the roll to roll nanoimprint lithography process, which is schematically depicted in detail in (b). The flexible large-are PDMS mold having the hole pattern shown in (c) is rolling over a epoxysilsesquioxane (SSQ)-coated Al/SiO_2/Al/PET substrate under conformal contact, imprinting the epoxysilsesquioxane (SSQ) dot pattern with a very thin residual layer as indicated in (d) [48]. 5

Figure 1. 3. Schematic of the designed Al wire grid polarizers embedded in Polydimethylsiloxane (PDMS)[30]. 7

Figure 1. 4. Triacetyl cellulose film are used as protection film of LCD's polarizer [46]. 8

Figure 2. 1. Chemical structure of bisphenol F-type epoxy resin (a) and NBR-based epoxy resin (b). 15

Figure 2. 2. Modulus (a), tensile strength (b), impact strength (c), and elongation (d) of the cured epoxy resin containing different mixing ratio of bisphenol F-type epoxy resin and NBR-based epoxy resin. 16

Figure 2. 3. SEM image of the nanopattern after first nanoimprinting. 18

Figure 2. 4. Schematic of the fabrication process of ultrasmall structures using ALD and a tunable UV curable epoxy resin. 20

Figure 2. 5. SEM image of the nanopattern after the ALD of alumina 21

Figure 2. 6. SEM images of the nanopattern after second nanoimprinting (a) Cross-section shape and (b) top view. 22

Figure 2. 7. SEM images of the nanopattern before (a) and after (b) RIE using O_2 24

Figure 2. 8. SEM images of the nanopattern after the reactive ion etching 25

Figure 3. 1. Angled deposition of aluminum on a nanopattern. 32

Figure 3. 2. The total process involved in the fabrication of WGP in this study. 33

Figure 3. 4. Simulation results for the WGPs that contain the different heights of the nanopattern (220 nm period, 70 nm linewidth, 30 nm thickness of aluminum). 35

Figure 3. 5. Simulation results for WGPs that contain Epoxy-SSQ nanopattern with 20 nm and 30 nm aluminum deposition on both the sidewalls. 36

Figure 3. 6. SEM photograph of SSQ nano pattern on a flexible PET film (a) and the cross section of a nanopattern after aluminum deposition and ion etching (b). 38

Figure 3. 7. Flexibility of a PET film containing WGP structure. 39

Figure 3. 8. The TE & TM curves of a nanopatterned Epoxy-SSQ WGP with 20 nm and 30 nm aluminum deposition on both the sidewalls. 41

Figure 4. 1. Simulation results showing the angle dependency for WGPs of 220 nm-period polymer grating [TM transmission (a) and TE transmission (c)], and by a 180 nm-period polymer grating [TM transmission (b) and TE transmission (d)]. The height of the nanograting is 200 nm, and the thickness of the aluminum coating on the grating sidewall is 20 nm. 50

Figure 4. 2. Double-angled evaporation of aluminum onto a nanopattern and the reactive ion etching process. 52

Figure 4. 3. (a) SEM image of an SSQ nanopattern on a flexible PET film, and the cross section of a nanopattern (b) after aluminum deposition and (c) after RIE. 53

Figure 4. 4. The TE and TM curves of a nanopatterned epoxy-SSQ WGP with 20 nm aluminum deposition on both sidewalls (180 nm period, 70 nm linewidth, 200 nm grating height). 54

Figure 4. 5. The transmission of TM light for (a) the 220-nm period WGP and (b) the 180-nm period WGP. 56

Figure 4. 6. The simulation data for the refractive index of the encapsulating material affects the TE transmission. Refractive indexes are black 1.0, red 1.5, and blue 2.0. 58

Figure 4. 7. The TE and TM curves of a nanopatterned epoxy-SSQ WGP after PMMA encapsulation. 59

Figure 4. 8. The refractive index of the polymerized epoxy-SSQ measured with an ellipsometer. 60

Figure 4. 9. Simulations of TM and TE with 4 μm encapsulation of PMMA. 61

Figure 4. 10. Simulations of TM and TE with 2 μm encapsulation of PMMA. 61

Figure 4. 11. Fabry–Perot resonance between aluminum gratings and PMMA. 62

List of Tables

Table 3. 1. Simulation results of transmission (%) of TM/TE polarized light at the different wavelength for the WGPs for different thickness of aluminum deposition................................. 36

Table 3.2. Measured optical transmission (%) of TM/TE polarized light through nanopatterned Epoxy-SSQ/aluminum WGPs at the different wavelength for the WGPs of different thickness of aluminum deposition on the SSQ grating sidewalls 40

Table 4.1. Measured optical transmission (%) of TM/TE polarized light through nanopatterned epoxy-SSQ/aluminum WGPs. 55

Abstract

In this dissertation, I report the development of a nanoimprint-lithography-based method of fabricating a wire grid polarizer (WGP), which greatly relaxes patterning and etching requirements and can be easily applied to produce flexible WGPs. Nanoimprinting is a simple and cheap large-area nanofabrication process. To date, WGPs were fabricated by electron beam lithography. Although electron beam lithography has a high resolution and good profile, it is slow and expensive. Therefore, electron beam lithography is not suitable for large-area nanofabrication. To fabricate larger WGPs, nanoimprinting lithography is one of the best processes.

Resists are very important materials used in nanoimprint lithography. WGP resolution and material brittleness have somewhat limited the choice of previous resists used for nanoimprinting. Hence, I developed an epoxy resist whose physical properties were tuned by adjusting the ratio of bisphenol F-type to acrylonitrile-butadiene rubber (NBR)-based epoxy resins in the resist formulation. The mechanical properties of the resist were tuned to obtain various aspect ratios and mold flexibility for conformal contact over nonplanar surfaces and large areas.

Roll-to-roll nanoimprint lithography is a very attractive method of manufacturing micro- and nanopatterns owing to its large-area patterning capabilities, high throughput, and low cost. Material flexibility is one of the most important requirements in roll-to-roll nanoimprint lithography. Commercially available bisphenol F-type epoxy resin is much less expensive than other resins, so it is a widely used construction polymer. NBR rubber is also widely used. Hence, the resist formulation I developed could be used to industrially mass-produce nanostructures. In addition, I used atomic layer deposition to fabricate 20-nm-linewidth, 9:1-aspect-ratio ultrasmall nanostructures. My method is faster and more economical than electron beam lithography.

I used nanoimprint lithography to pattern a high-aspect-ratio, narrow-linewidth grating and subsequently deposited two aluminum layers angled in opposite directions to efficiently fabricate the large-area WGP. Anisotropic reactive-ion etching was used to remove the aluminum layer deposited on top of the grating while retaining that on the grating sidewalls, thereby forming a metal wire grid whose spacings were much smaller than those of a lithographically defined grating. The WGP showed good optical properties in the visible range. I encapsulated the WGP in a thin layer of poly(methyl methacrylate) (PMMA) for practical use, and the encapsulated WGP worked well in the visible range.

Chapter 1

Introduction: background of nanoimprint lithography and polarizer

1.1. Motivation of nanoimprint lithography

Various methods of fabricating and tuning nanostructures are becoming increasingly important as industry develops. Regular, well-ordered nanostructures are being widely studied because they can be used in various applications. The structures whose patterns are <100 nm are called “nanostructures.” Electron beam lithography is one of the most widely used methods of fabricating nanostructures [5, 10, 20, 74, 91]. Conventional electron beam lithography limits nanostructure feature size to 8 nm [23]. Attempts have recently been made to fabricate nanostructures showing 5 nm feature size [60]. However, electron beam lithography is slow, and not only the electron beam lithography tool but also its maintenance are expensive [19]. Thus, electron beam lithography is unsuitable for large-area nanofabrication. Nanoimprint lithography was subsequently invented to overcome these disadvantages.

1.2. Nanoimprint lithography

Nanoimprint lithography is an emerging technology that promises high-throughput nanostructure patterning. It is currently being used to fabricate electronic devices, biological nanosensors, and optical devices. The principle of nanoimprint lithography is quite simple. Nanofeatures are defined on the surface of a hard mold, which is used to emboss them into a polymer cast onto a wafer substrate under controlled temperature and pressure [35]. Although polymers were initially molded during early nanoimprint lithography development, monomers have been recently used in nanoimprint lithography. And the monomers were polymerized during the process of nanoimprint lithography [7, 52, 90]. Comparing the nanostructures produced using numerous polymers and monomers has shown that detailed nanostructures can, in fact, be fabricated using monomers. But when monomers are used in nanoimprint lithography, the volume of the nanostructures are reduced during polymerization [79], thereby making it difficult to control the exact size of nanoimprint-lithography-fabricated nanostructures. Prepolymers could be used instead of monomers during nanoimprint lithography, which requires using many materials showing various physical properties to imprint a diverse range of nanostructures. I will introduce nanoimprint lithography materials whose physical properties can be tuned simply by changing the ratio of the mixture components. Furthermore, I will introduce a method of fabricating smaller nanostructures.

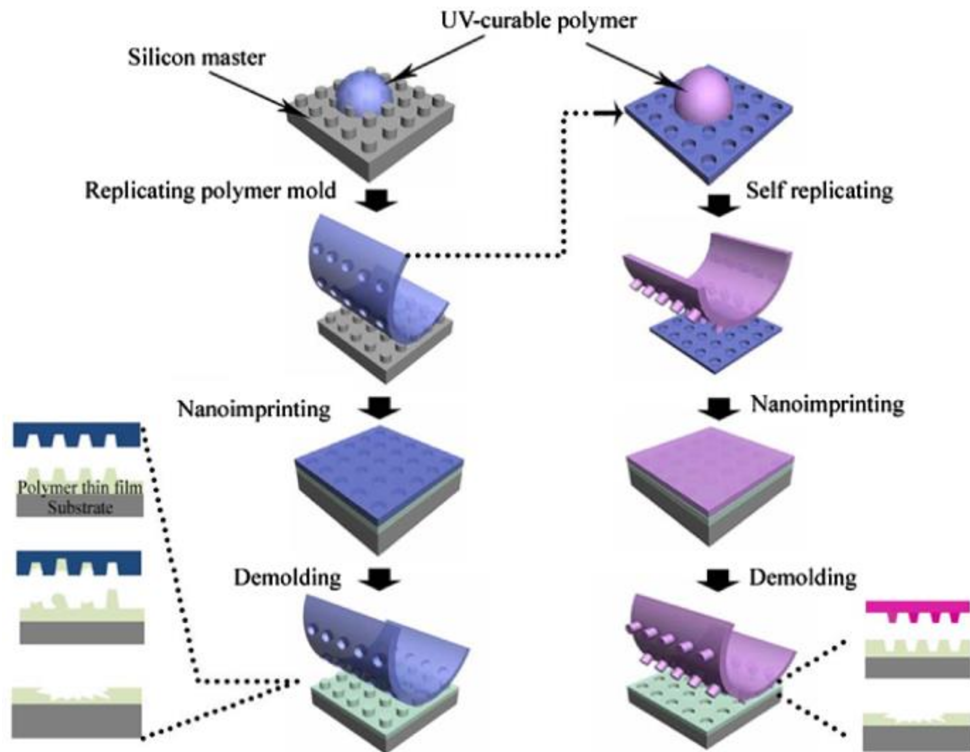

Figure 1. 1. Schematic illustrating nanopattern fabrication by soft nanoimprinting with flexible molds. Left and right columns show patterning dense dot and hole arrays, respectively, from complementary molds. Left and right bottom panels show some demolding failures[47].

1.2.1. Nanoimprint lithography materials

Using appropriate materials is the key in nanoimprint lithography because they determine which curing methods are used. For example, polydimethylsiloxane (PDMS) is commonly used because of its flexibility and low surface energy. However, it shows high viscosity—SYLGARD® 184 (Dow Corning) = 3900 mPa s—thus, the material flow limits the fabrication process resolution for sub-100-nm pattern geometries [50, 54, 101]. Further, its relatively low Young's modulus can

lead to structural problems in pattern-transfer elements, especially for high-aspect-ratio nanostructures [14].

Thermoplastic polymers have been widely used as resist layers for nanoimprint lithography [80]. However, such polymers show very high viscosities even when heated above their glass transition temperatures (T_g). Consequently, fabricating high-aspect-ratio nanostructures typically requires high pressures and long imprinting times, which considerably decreases throughput. Hence, using photocurable materials, which can be imprinted at room temperature, is preferred for nanopatterning to achieve the high throughput required for high-volume industrial nanofabrication [37].

To resolve the issues, the photocurable epoxysilsesquioxane (SSQ) resins were synthesized and they were used as functional patterning layers in high-resolution, large-area nanoimprint-lithography applications [77]. Incorporating photocurable epoxy groups enables nanoimprinting to be completed within seconds at room temperature, and the phenyl groups enhance the Young's modulus of the material [77]. However, cured SSQ is too brittle, so we developed a nanoimprint resist flexible enough to fabricate high-aspect-ratio nanostructures.

1.2.2. Roll to roll nanoimprint lithography.

The roll-to-roll nanoimprint lithography was used to continuously fabricate large-area nanopatterned structures in order to further scale processing [4, 43, 44, 69, 93, 99]. In roll-to-roll nanoimprint lithography, a flexible nanostructured mold wrapped around a roll makes contact with another roll to which a substrate coated with UV-curable resist is attached and produces a

nanopattern as the rolling proceeds under slight pressure and UV curing to crosslink the resist [61, 70, 85].

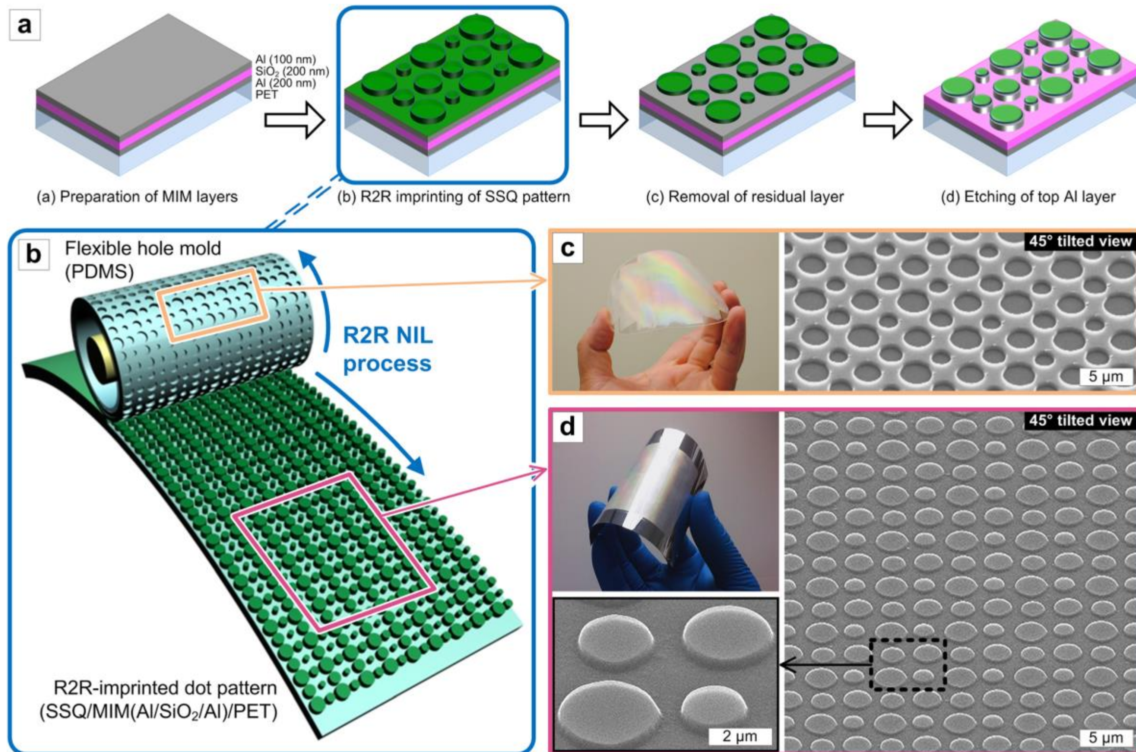

Figure 1. 2. (a) Illustration of overall metal-insulator-metal (MIM)-based nanostructure fabrication. Roll-to-roll nanoimprint lithography, schematically depicted in detail in (b), was used to continuously transfer SSQ pattern onto MIM-deposited polyethylene terephthalate (PET) substrate. Flexible large-area PDMS mold showing hole pattern (c) is rolled over conformally contacted SSQ-coated Al/SiO_2/Al/PET substrate, imprinting SSQ dot pattern with very thin residual layer (d) [70].

1.3. Motivation of fabricating wire grid polarizer

Polarizers are widely used in display technologies. Wire grid polarizers (WGPs) consist of subwavelength periodic metal lines [48, 86, 98]. The WGP polarization spectrum corresponds to the periodic spacing of the metal lines. Early WGP nanopatterns were periodically spaced >1 μm apart because nanotechnology was not well developed; therefore, early WGPs were used to polarize infrared light [9]. The periodic spacing of visible light polarizers should be hundreds of nanometers. WGPs can currently be fabricated using electron beam lithography, which is slow and very expensive. Hence, WGPs do not commercialize well for display applications even though they are more efficient and compact than conventional polarizers [6]. I used nanoimprint lithography with relaxed conditions, which enables large-area WGPs to be economically fabricated.

1.3.1. WGP principle

A WGP consists of a grid of parallel wires, which reflect one polarization of incident electromagnetic radiation while transmitting another. The grid period should be smaller than half the incident light wavelength [102]. In other words, the transverse electric (TE) field running along the direction of a metal wire induces free electrons to move along the wire because light is composed of electromagnetic fields. Thus, the polarized light is reflected similar to light reflecting from a metal surface. However, electrons cannot traverse very far between metal wires when incident light is used to apply an electric field perpendicular to the wires, so a transverse magnetic (TM) field is transmitted through WGPs [40].

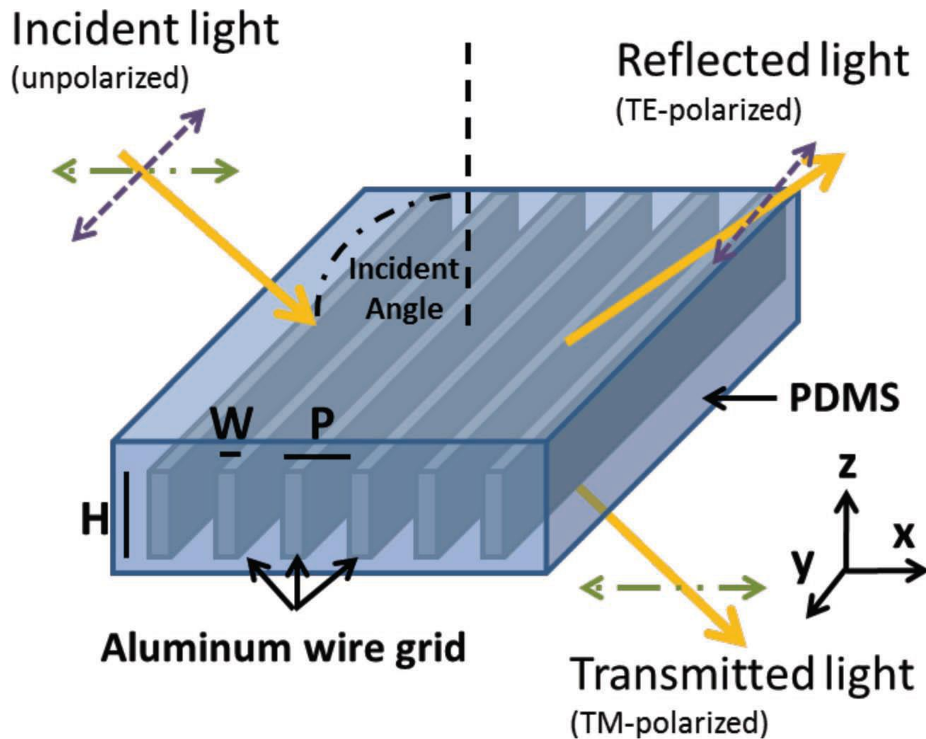

Figure 1. 3. Schematic of designed Al WGPs embedded in PDMS [40].

1.3.2. Conventional polarizers

Conventional polarizers are most commonly fabricated by treating polyvinyl alcohol chains with iodine and subsequently annealing the chains to stretch and align them [34]. The resulting iodine/polyvinyl alcohol chains appear as atomic-scale WGPs. The electrons on iodine can move parallel to the aligned polyvinyl alcohol chains but cannot traverse the chains. However, conventional polarizers absorb 60% of the incident light [30]. The optical efficiencies of displays are very important, so WGPs could be good candidates to prevent absorption loss. Conventional polarizers must also be coated with a hydrophobic protection layer because polyvinyl alcohol easily dissolves in water. Fabricating thin conventional polarizers is difficult because the

protection layer is thick. A widely used protection layer is ~200-μm-thick triacetyl cellulose film [67]. Further, iodine polarizers are not durable under harsh conditions because iodine sublimates [59]. Recent research has focused on substituting the iodine with dye molecules [38], and WGPs simply fabricated using nanoimprint lithography are one of the best substitutes for iodine polarizers.

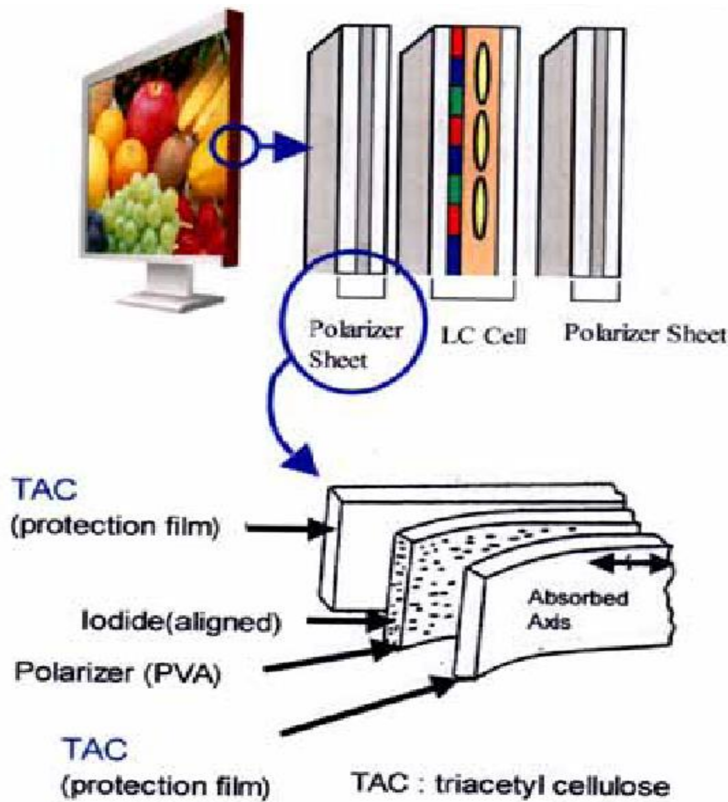

Figure 1. 4. Triacetyl cellulose films used to protect liquid crystal display (LCD) polarizer [67].

Chapter 2

Nanoimprinting ultrasmall and high-aspect-ratio structures by using rubber-toughened UV cured epoxy resist

2.1. Introduction

The ability to fabricate and manipulate nanostructures has played an important role in modern science and technology, especially for electronic, optical, and nanoelectromechanical devices, and nanometer-scale biological sensors [36, 49, 76, 77, 84]. Conventional methods, such as photolithography and electron-beam lithography, used for fabricating nanostructures [66] are generally too costly to be suitable for many applications. Unconventional methods, such as nanoimprinting and soft lithography, provide simpler and cheaper alternative routes for nanoscale fabrication. Both nanoimprinting and soft lithography are parallel processes in which various patterns are simultaneously formed by the physical contact of a hard or soft mold with the targeted substrate.

The imprint lithography based on a hard and rigid master mold can provide resolutions down to a few nanometers. However, it requires extremely flat surfaces or very high pressures for conformal coating of the substrate [18]. The soft lithography technique, based on a soft mold typically made of PDMS, does not necessarily require high pressure or a flat surface. However, its resolution capability is limited [25, 51, 56]. Additionally, in the sub-micrometer range, the PDMS mold loses its mechanical integrity and deforms into unexpected shapes [21, 42].

In order to overcome these problems, several approaches such as the step and flash method by using a relatively small area mold [8], low-pressure nanoimprint lithography using the fluoropolymer [46], utilizing modified PDMS [29, 68, 81], or alternative materials in soft lithography [75, 92] have been considered. Nevertheless, certain basic problems such as the requirement of an expensive quartz mold in the step and flash imprinting, relatively long processing time in the low-pressure imprinting, and pattern collapse in soft lithography when the features are fine and dense with a high aspect ratio, were found. As these problems were inherently related to the mold material, there was a need to engineer new imprint molds that can provide high rigidity sufficient for fine and dense features with a high aspect ratio and an additional degree of flexibility for the conformal contact over non-planar and large area surfaces.

UV nanoimprinting is most desirable from the processing speed point of view. Cationic polymerization is preferred for UV nanoimprinting as free-radical polymerization suffers from oxygen inhibition [36]. Moreover, as epoxy functional groups can be polymerized through the cationic ring opening polymerization, many monomeric compounds having epoxy functional groups have been exploited in nanoimprinting research [2, 3, 15, 45, 58, 73]. All the synthesized compounds have distinct physical properties such as modulus and tensile strength after curing, and thus, when a different physical property is needed, the modification of epoxy functional

compounds is difficult.

Epoxy resins constitute one of the most important classes of thermosetting polymers, and they have been extensively used as high-performance adhesive composite materials due to their outstanding mechanical and thermal properties such as high modulus and tensile strength, low creep, high glass transition temperature, high thermal stability, and moisture resistance [87]. However, in the cured state, epoxy resins are brittle and have fracture energies approximately two orders of magnitude lower than those of engineering thermoplastics. In order to endure the strong mechanical stress during mold separation, it is important to increase the fracture energy so that the integrity of the imprinted resist patterns can be maintained. One of the most successful methods to toughen epoxy resins is the incorporation of a rubber phase into the brittle epoxy matrix. This is achieved through incorporating reactive liquid rubber or preformed rubber particles with reactive functional end groups such as carboxyl, amine, or epoxy [12, 27, 57, 63, 78].

In this study, a new resist formulation for nanoimprinting using a similar strategy of introducing rubber-containing moieties into the epoxy resist formulation is considered. The method is capable of tuning the properties of epoxy resins from hard to soft by adjusting the ratio of bisphenol F-type epoxy resin and acrylonitrile-butadiene rubber (NBR)-based epoxy resin in the formulation of resist. Additionally, a simple and easy method to fabricate the high-aspect-ratio structures and the ultrasmall structures by two consecutive nanoimprintings with atomic layer deposition (ALD) [31] to narrow the trench width of the mold patterns is introduced. The residual layer of the imprinted pattern can be easily removed using standard oxygen-based reactive ion etching (RIE), and the pattern can be transferred into a silicon substrate by using the remaining nanopattern as a mask. Compared with previously developed SSQ resist [76, 77], the

new material offers a distinct advantage in that the Si or silica mold can be cleaned by O_2 plasma treatment without affecting the mold structures.

2.2. Experimental

2.2.1. Materials and instruments

1H,1H,2H,2H-perfluorodecyltrichlorosilane was purchased from Gelest and bisphenol F-type epoxy resin (YDF-170) and NBR-based epoxy resin (R-1309) were purchased from Kukdo Chemical (Korea). Propylene glycol monomethyl ether acetate (PGMA) and triarylsulfonium hexafluoroantimonate salt (50 wt% in propylene carbonate) were purchased from Aldrich Chemical. The triarylsulfonium hexafluoroantimonate salt was used as a photoacid generator (PAG). The modulus and tensile strength were measured using a universal testing machine (Instron5944), and the samples of the materials were formed as films. A Nanonex imprinting tool (NX2000) with vacuum capability and UV curing system was used for the nanoimprinting. ALD was performed by OpAL (Oxford Instruments) [22], and an IR spectrum was obtained from the IFS 66/S (Bruker Optics). The curing was monitored using the IR spectrum obtained before and after the curing of nanoimprinting. In order to estimate the toughness and impact strength of the rubber-modified epoxy polymer, the material was measured by using an Izod impact tester (IM-705C) according to ASTM D256. A minimum of six specimens were tested, and the average results were recorded.

2.2.2. Nanoimprinting of modulus-tunable UV cure epoxy resist

An original silicon oxide master mold was vapor-coated with 1*H*,1*H*,2*H*,2*H*-perfluorodecyltrichlorosilane in order to achieve easy mold release after the imprinting and curing process**.** The nanoimprint resist formulation was made by dissolving the bisphenol F-type resin and NBR-based epoxy resin in PGMA, and was followed by the addition of the PAG (3.0 wt% to the epoxy resin). The concentration of the resist solution was adjusted by adding more solvent so that the thin film thickness (from micrometers to nanometers) could be readily obtained by spin coating. The imprinting pressure was typically less than 50 psi due to the low viscosity of the epoxy resist. Although 1 min was sufficient to cure the epoxy resin, additional time was needed for the epoxy resin, which contained the NBR-based epoxy resin. However, the speed of curing could be increased by considering higher PAG concentration.

2.2.3. Atomic Layer Deposition (ALD)

ALD is a thin-film deposition technique that is based on the sequential use of a gas-phase chemical process. As the ALD process deposits precisely one atomic layer in each cycle, complete control over the deposition process is obtained at the nanometric scale. A process with alternating steps of trimethylaluminum and H_2O dosing in OpAL (Oxford Instruments) was carried out. The first step is trimethylaluminum dosing for 20 ms followed by 4 s purging of the trimethylaluminum precursor. The next step is H_2O dosing for 20 ms with 50 sccm Ar. The H_2O dosing step hold time is 4 s with a total cycle time of 8 s. The growth rate is 1 A/cycle, and in order to grow 20-nm thickness of alumina, the total number of cycles required is 200. All the depositions are performed

at a relatively low temperature of 150 °C. Using ALD, the conformal coating can be achieved even with high aspect ratio and complex structures.

2.2.4. Reactive ion etching (RIE)

LAM 9400 (LAM Research Corporation, CA, USA) was used for RIE. In order to remove the residual layer, RIE was conducted in the presence of O_2. The applied pressure was 12 mTorr. The TCF RF was 100 W, and the bias RF was 30 W. The flow rate of O_2 was 20 sccm, and the etching time of 10 s was required to remove the 25 nm residual layer. RIE was performed with Cl_2 in order to remove the SiO_2 on the silicon wafer. The pressure in this RIE process was 12 mTorr, and the TCP RF was 300 W. The bias RF was 50 W, and the flow rate of Cl_2 was 30 sccm. The etching time required was 5 s. In order to remove the silicon part on the silicon wafer, RIE was conducted with HBr and He. The pressure in the RIE process was 12 mTorr, the TCP RF was 500 W, and the bias RF was 30 W. The flow rate of HBr was 100 sccm, while that of He was 100 sccm.

2.3. Results and discussion

2.3.1. Tuning Physical Property of Resist

The use of resist materials for nanoimprinting results in specific mechanical properties. However, it is desirable to tune the hardness or flexibility of the resist for different applications. In this study, two kinds of epoxy resins—bisphenol F-type epoxy resin and acrylonitrile-butadiene

rubber (NBR)-based epoxy resin—are used for nanoimprinting. Bisphenol F-type epoxy resin was used as a basic epoxy resin material, and NBR-based epoxy resin was added for the increased flexibility of the finally cured epoxy material. The chemical structures are shown in figure 2.1. The physical property of the epoxy resist is modulated by changing the mixing ratio of the epoxy resins. It is very important to achieve homogeneity of the mixture when more than two kinds of epoxy resins are mixed. Thus, a mechanical stirrer was used for more than 40 h to ensure adequate mixing. A sulfonium salt was used as the initiator for UV curing of the mixed epoxy resins.

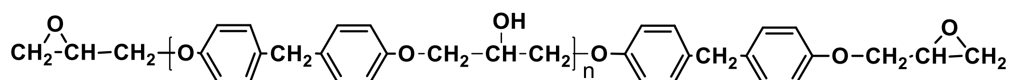

(a)

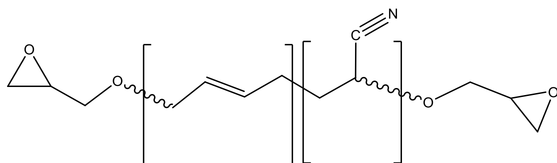

(b)

Figure 2. 1. Chemical structure of bisphenol F-type epoxy resin (a) and NBR-based epoxy resin (b).

Prior to nanoimprint study, important mechanical properties such as the modulus, the tensile strength, and the impact strength of the cured epoxy resins were measured for materials with different mixing ratios of the epoxy resins, and the results are summarized in figure 2.2.

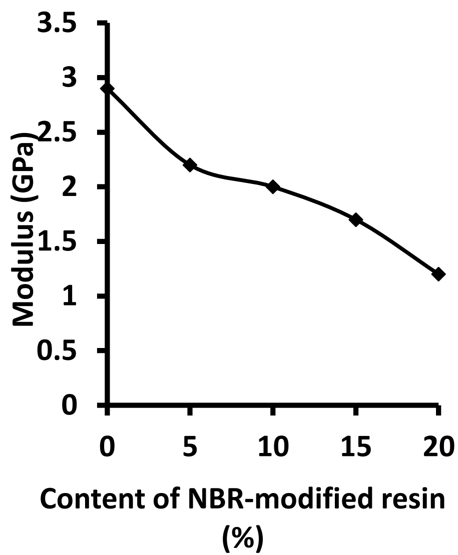

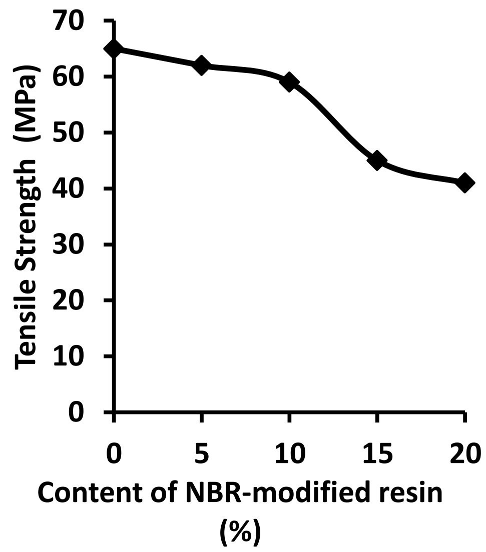

(a) **(b)**

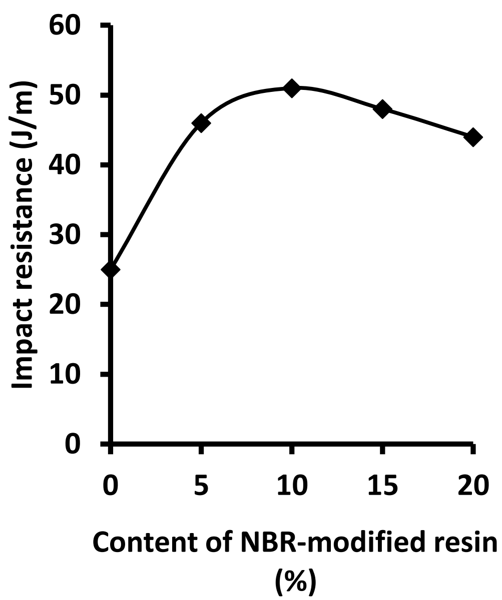

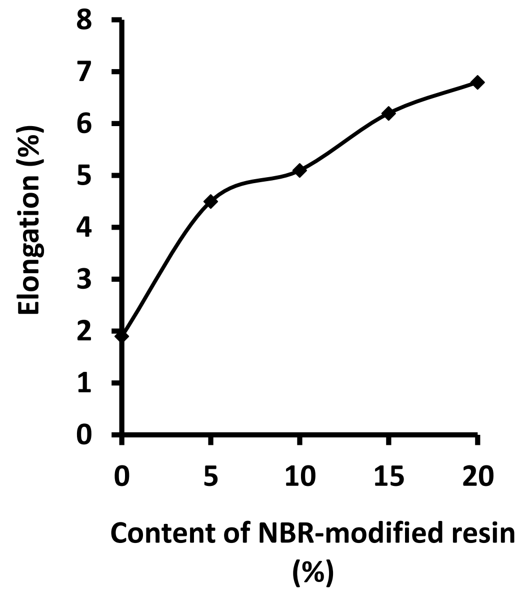

(c) **(d)**

Figure 2. 2. Modulus (a), tensile strength (b), impact strength (c), and elongation (d) of the cured epoxy resin containing different mixing ratio of bisphenol F-type epoxy resin and NBR-based epoxy resin.

From analysis of figure 2.2(a), it is apparent that we can control the modulus from 2,900 MPa to 1,200 MPa by changing the NBR-based epoxy resin mixing ratio from 0 % to 20 %, thus allowing the preparation of a range of materials from hard to soft. In figure 2.2(b), it can be seen that the tensile strength decreased with an increase in the mixing ratio of the NBR-based epoxy resin. A less rigid material maintaining sufficient modulus and tensile strength is advantageous to create a mold for nanoimprinting as it can increase the yield during the demolding process and can be ideal raw materials for good flexible mold for the roll-to-roll nanoimprinting process [2, 3]. Impact strength is one of the important physical properties for estimating the toughness of the polymer. The impact strength of the epoxy polymers used in this study was estimated by the Izod method. In figure 2.2(c), the impact strength of the epoxy polymer (YDF-170) was 25 J/m, and this impact strength was increased sharply to 51 J/m by addition of a small amount of the NBR-modified epoxy resin (R-1309). Addition of more than 10 % of R-1309 slightly decreased the impact strength. The sharp increase represented twice the impact strength of some of the thermoplastic materials commonly used for nanoimprinting, e.g., poly(methyl methacrylate) [PMMA] (~27 J/m) and polystyrene (~28 J/m). Some of the highest-aspect-ratio structures were imprinted into PMMA [36]. In addition, mixing the NBR-based epoxy resin to the bisphenol F-type epoxy resin results in the most important change, i.e., several-folds increase in the elongation at break. In figure 2.2(d), the elongation of the epoxy polymer (YDF-170) was only 1.9 %, while the elongation increased sharply to 6.8 % due to addition of the 20 % NBR-modified epoxy resin (R-1309). The increase in elongation is closely connected to the toughness of the polymer. In this system, even though the decrease in tensile strength is connected to a decrease in the toughness, as the extent of elongation increase is much larger than the extent of decrease in tensile strength,

the toughness of the epoxy polymer increases with an increasing mixing ratio of the NBR-modified epoxy resin in the range of this experiment.

2.3.2.Nanoimprinting with silicon dioxide mold using the epoxy resins

Nanoimprinting was performed with a silicon dioxide mold (180 nm period, 60 nm line width, and 180 nm height) using different mixing ratios of the epoxy resin so as to obtain various nanoimprinted molds with diverse physical properties. The SEM image of the nanoimprinted pattern using epoxy resin [with mixing ratio 85: 15 (YDF-170: R-1309)] is shown in figure 2.3.

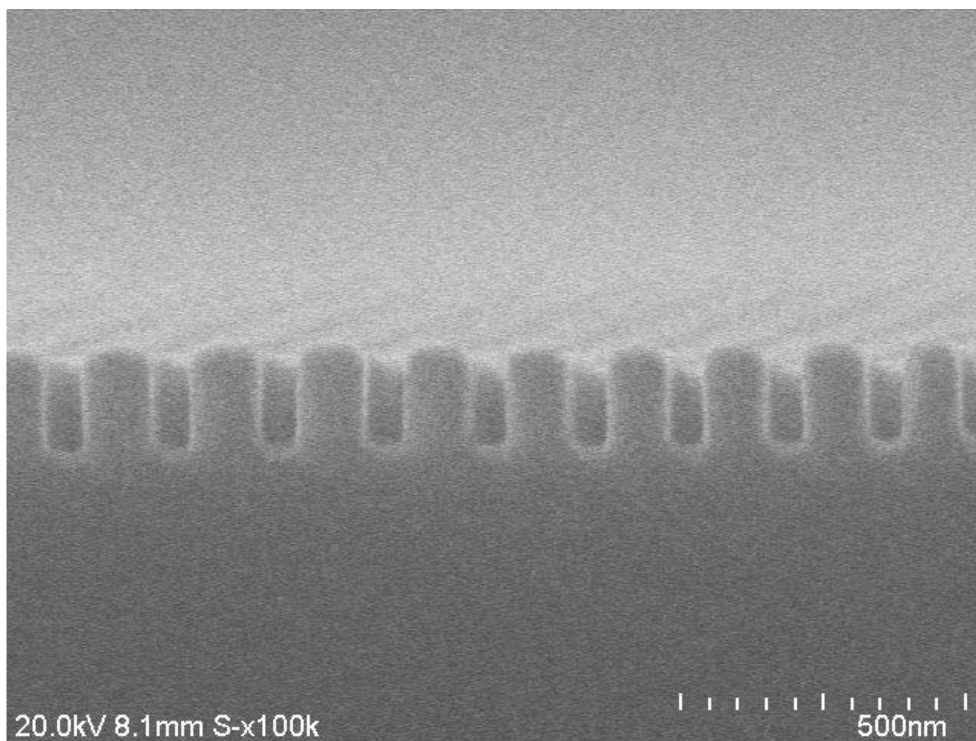

Figure 2. 3. SEM image of the nanopattern after first nanoimprinting.

In Figure 2.3, the SEM of nanopattern of mold with 180 nm period, 120 nm line width, 60 nm

trench, and 180 nm depth is shown. This epoxy resin is softer and tougher than the epoxy resin that is generally used in nanoimprinting. Therefore, the handling of this epoxy resin was easier than that of other epoxy resins; more importantly, large-area imprinting at the non-flat surface was greatly facilitated by the conformal contact between the mold and the imprinting material, which was enabled by the mechanical flexibility of the system.

The curing of epoxy resin was monitored by IR spectrums that were obtained before and after nanoimprinting. The IR spectra shows increased hydroxyl group (3,418 cm^{-1}) absorption, ether linkage (1,111 cm^{-1}) absorption, and the reduction in epoxy rings (914 cm^{-1}) absorption, confirming the polymerization through epoxy ring opening.

2.3.3. Reducing the trench of the nanopattern

A process for fabricating the ultrasmall structures with high aspect ratios through two consecutive nanoimprint processes with ALD so as to reduce the line width of the imprinted mold is developed in this study. The schematic of this process is shown in figure 2.4.

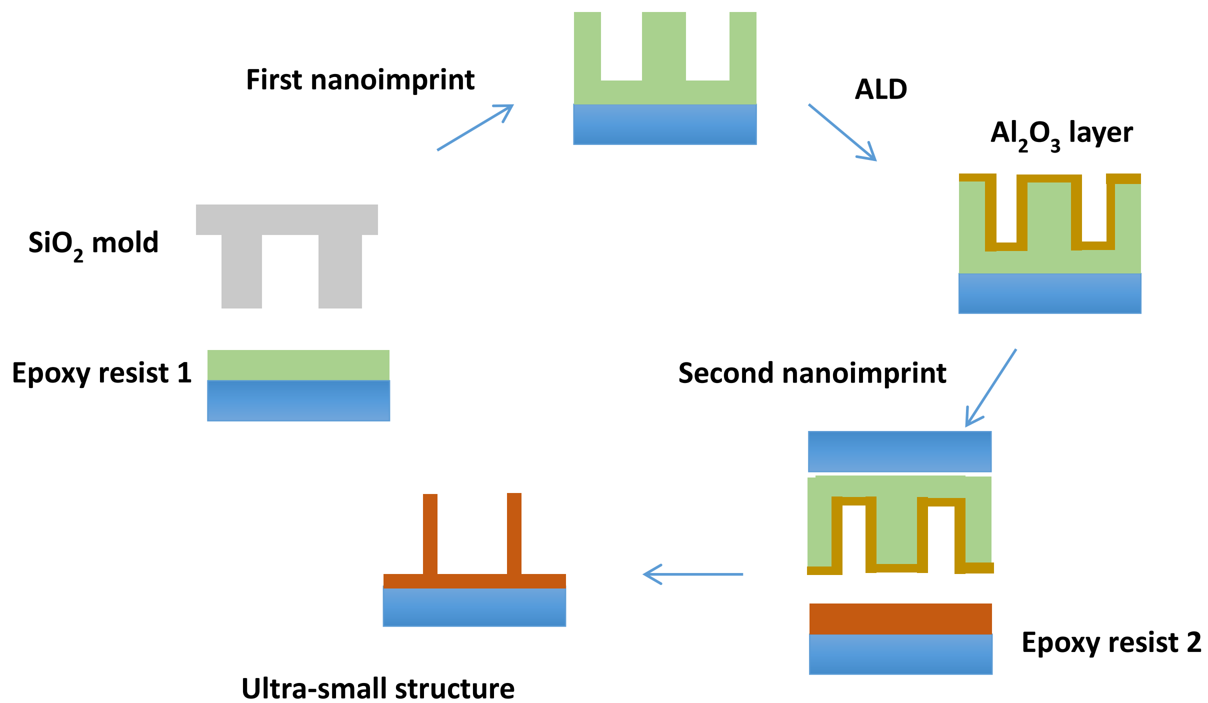

Figure 2.4. Schematic of the fabrication process of ultrasmall structures using ALD and a tunable UV curable epoxy resin.

During the ALD, Al_2O_3 is deposited at the rate of 20 nm/h. The SEM image result of the ALD of the structure with 180 nm period, 160 nm line width, 20 nm trench, and 180 nm depth is shown in figure 2.5. The trench of the nanopattern was reduced from 60 nm to 20 nm using the ALD.

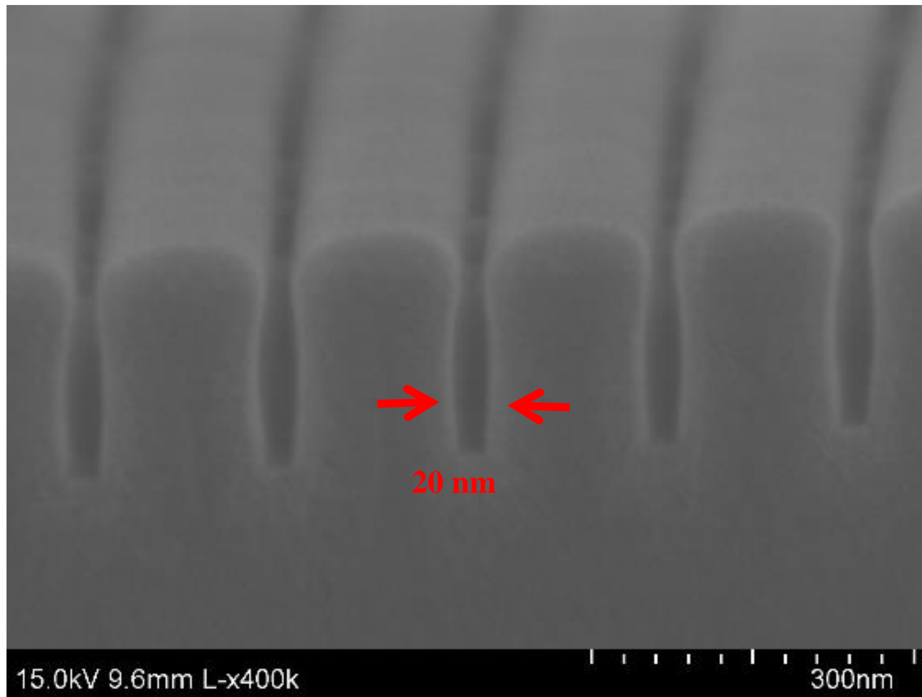

Figure 2.5. SEM image of the nanopattern after the ALD of alumina

2.3.4. Nanoimprinting to get the 20-nm-line-width nanopattern

Using this alumina-coated structure as a mold, nanoimprinting was carried out, and the final nanopattern was obtained with a structure with 180 nm period, 20 nm line width, and 180 nm height, leading to an aspect ratio of 9:1, which is among the highest ever reported. Taking advantage of increased impact strength by mixing the epoxy resins with ratio of YDF-170: R-1309 = 95: 5, the result showed the finest-structured nanopattern amongst all previous results. The SEM image of this nanopattern is shown in figure 2.6.

It is concluded that using the epoxy resin YDF-170: R-1309 = 85: 15 at the first nanoimprinting and using the epoxy resin YDF-170: R-1309 = 95: 5 at the second nanoimprinting is the best method for obtaining the fine nanoimprinted structure. Additionally, the process was successfully

applied without any difficulties, and good results were obtained for larger areas (2 in × 2 in).

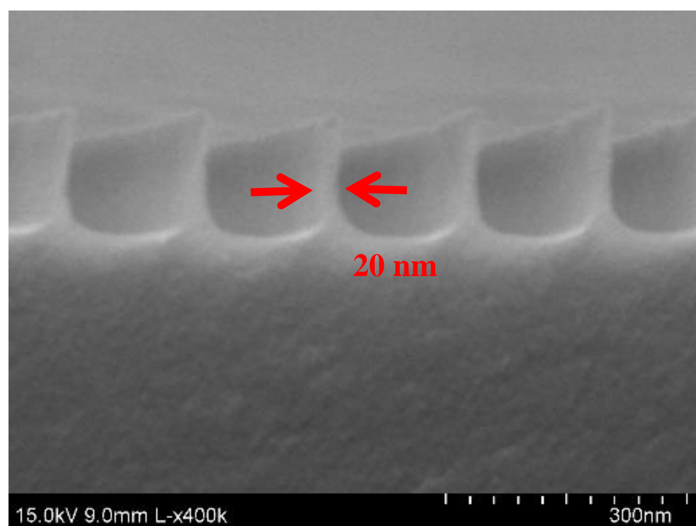

(a)

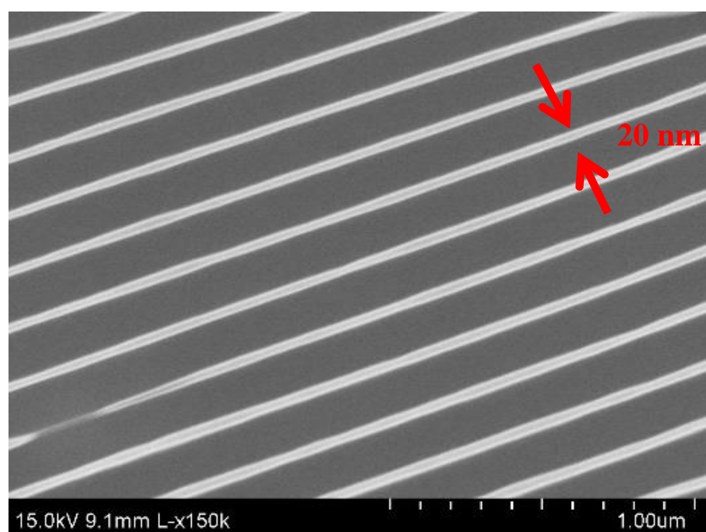

(b)

Figure 2.6. SEM images of the nanopattern after second nanoimprinting (a) Cross-section shape and (b) top view.

2.3.5. Reactive ion etching (RIE)

After conducting the nanoimprinting process, the average thickness of the residual layer was determined to be 25 ± 2 nm. In order to remove the residual layer, RIE was performed using O_2, and the etching rate was 3 nm/s.The SEM images for the cross section of the nanopattern before and after conducting RIE are shown in figure 2.7.

The cross section of the residual layer before conducting RIE is shown in figure 2.7 (a). The residual layer removed after conducting RIE using O_2 is shown in figure 2.7 (b).

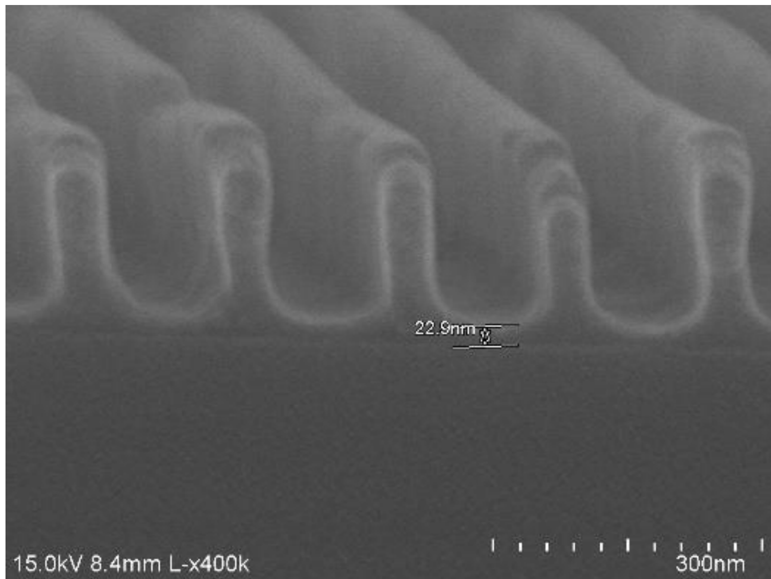

(a)

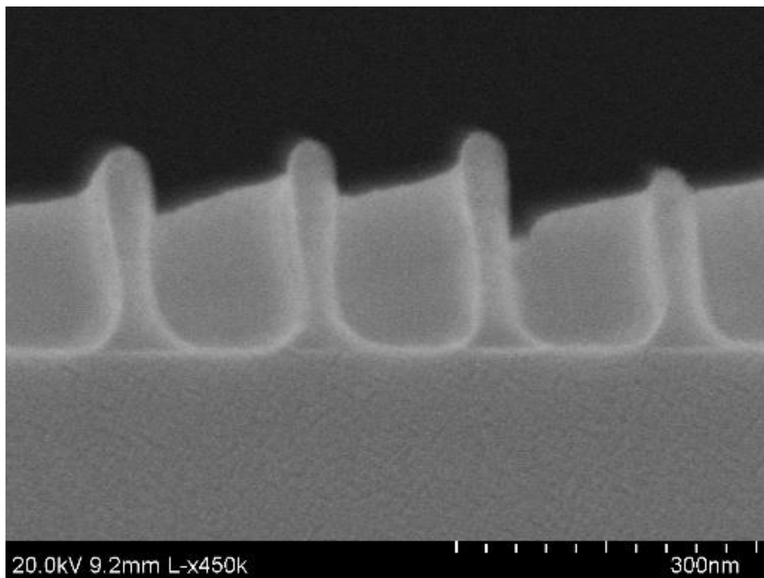

(b)

Figure 2.7. SEM images of the nanopattern before (a) and after (b) RIE using O_2

Pattern transfer into Si substrate by RIE was performed in order to show that the new resist system acts as a good etching mask for general microfabrication and nanofabrication purposes.

The remaining nanopattern could be used as an etching mask on removal of the residual layer. The native oxide on silicon wafer was removed using RIE with Cl_2. Subsequently, silicon was etched using RIE with HBr. The SEM image for the cross section of the nanopattern obtained on completion of the etching process is shown in figure 2.8.

As shown in figure 2.8, after the etching process, the mask's height was reduced to 100 nm, and 100 nm depth of silicon part was etched. 100 nm depth of the silicon wafer is etched, and the mask's height was only reduced a little in this process, leading to a selectivity of 1:1 (resist to Si). This shows that the new resist formulation can be used as a mask for semiconductor processing.

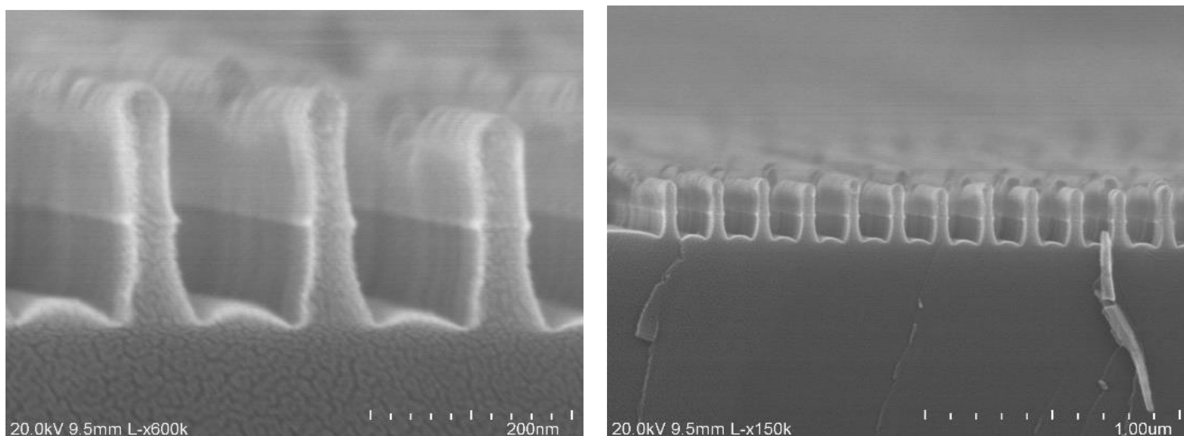

Figure 2.8. SEM images of the nanopattern after the reactive ion etching

2.4. Conclusions

Thus an easy and simple method to fabricate ultrasmall structures by two consecutive nanoimprintings with ALD using the tunable UV cure epoxy resin is introduced in this study. The epoxy resin was composed of bisphenol F-type resin and NBR-based epoxy resin. The modulus of the cured epoxy polymer was controlled by changing the mixing ratio of the two epoxy resins. The impact strength of the epoxy polymer was sharply increased to 51 J/m via addition of the NBR-modified epoxy resin. A nanopattern with a trench size of 60 nm was obtained after the first nanoimprinting. The size of the trench was then reduced to 20 nm using the ALD technique. Using this pattern as a mold, a 20 nm ultrasmall structure and a high-aspect-ratio (9:1) structure was finally obtained. This technique could also be used for larger size molds (more than 2 in × 2 in). Using RIE with O_2, the residual layer in the nanopattern was removed. The silicon wafer was etched using RIE with HBr and He using the remaining nanopattern as a mask. This result showed that the resist in this study could be used in semiconductor process.

Chapter 3

Facile route of flexible wire grid polarizer fabrication by angled-depositions of aluminum on two sidewalls of an imprinted nanograting

3.1. Introduction

A polarizer is an essential optical device for many optical systems and networks such as polarization-based imaging systems, free-space optical switching networks, and fiber-optic networks. Conventional polarizers are bulky optics and may not be suitable for certain applications. A metal wire grid is a potential candidate for making a high-quality, integration-capable, thin-film-type polarizer [1, 32, 55, 71, 72, 95-97]. Wire grid polarizers (WGPs) offer a large spectral working range, small feature size and good integrability. WGPs are important for various applications such as microscopy or imaging systems, and can also be used as polarized beam splitters.

Using a WGP to replace the traditional polarizing film in LCDs can improve the LCD brightness as little light is absorbed by WGPs and reflected light can be recycled. Generally, a WGP consists of a periodical arrangement of conductive (metallic) wires on a transparent substrate. Upon illumination, a wire grid polarizer transmits light with an electrical field vector perpendicular to the wires (transverse magnetic (TM) polarization) with high efficiency, and reflects the parallel counterpart (transverse electric (TE) polarization). In addition to the transmission of TM-polarized light, the extinction ratio, which is defined by the transmission ratio of TM- and TE-polarized light, is another characteristic optical property of a wire grid polarizer. The spectral working range and the optical properties of a wire grid polarizer (such as transmittance and extinction ratio) are determined by the grating material and the structural parameters of the metal grating such as the period, grating height, and linewidth.In the last two decades various research results on the fabrication of WGPs using NILs were reported [1, 32, 55, 71, 72, 95-97]. Ekinci et al. have demonstrated the realization of a new bilayer metal WGP [24]. They fabricated the bilayer metal WGP by evaporating an aluminum film onto a poly(methyl methacrylate) resist grating fabricated using interference lithography. Hsu et al. have described the fabrication process of a flexible nano-wired polarizer by contact-transferred and mask embedded lithography using a polyurethane acrylate mold [41]. To pattern the fine pitch required for WGP, nanoimprint lithography (NIL) has been used in recent years due to its potential for high resolution and high throughput nanoscale patterning [15-17, 36]. Previously we reported the fabrication of bilayer metal WGPs on flexible plastic substrates by roll-to-roll UV nanoimprint lithography using an epoxysilicone resist [13] and metal evaporation technique [2]. The high-throughput UV-NIL process has the potential to enable large area metal WGPs fabrications [2, 13].

Displays have progressed toward increasingly thinner, lighter weight, and more flexible devices

over the last few years. This is especially true in the field of mobile devices. Polarizers made on polymer substrate could find applications in future flexible LCD displays. WGPs require fabrication of subwavelength metal gratings, which presents a significant challenge for patterning and etching of dense structures, particularly for use in visible wavelength applications. This becomes even more challenging to process on a flexible substrate. It is known that the WGP should have a period lower than 150 nm in order to provide adequate bandwidth to cover the visible light range. In this study, a flexible WGP was fabricated on a poly(ethylene terephthalate) (PET) film by using a new method with the nanoimprint lithography (NIL). Even though the imprinted high aspect ratio grating has a relatively large 220 nm period, the WGP obtained using the new method still showed very good performance in the wide visible band of the spectrum. This is made possible by using double angled aluminum deposition to cover the sidewalls of the imprinted polymer grating, therefore much narrow spacing between the aluminum lines have been obtained. An isotropic reactive ion etching was then used to selectively remove the aluminum deposited at the top of the grating, thereby forming metal wire grids with much smaller spacing than lithographically defined gratings. This new approach significantly relaxes the stringent requirement for the fine line patterning process used in traditional methods, and is especially desirable for future manufacturing of flexible WGPs using roll to roll nanoimprint process.

3.2. Experimental

NIL was performed on a flexible PET film in order to fabricate a flexible WGP. A nanograting of 220 nm period, 70 nm linewidth, and 200 nm height was imprinted into epoxy-silsesquioxane material. As compared with the material reported [77], the epoxy-silsesquioxane

used in this work was synthesized by using a larger amount of fluorinated compound to achieve higher aspect ratio structures. Then, two angled aluminum depositions were performed from both sides of the grating walls at 40 degree angle from a normal direction. Aluminum from the upper part of the pattern was removed by reactive ion etching. The obtained WGP had a unique structure in which aluminum coatings were on both sides of the wall of the nanopattern, creating a flexible WGP on PET.

3.2.1. Materials and synthesis of SSQ

To synthesize the SSQ material, phenyltrimethoxysilane (PTMS), (3-glycidyloxypropyl)trimethoxysilane (GTMS), (tridecafluoro-1-octyl)triethoxysilane (FTES), CsOH, propylene glycol monomethyl ether acetate (PGMA), were purchased from Aldrich Chemical (St. Louis, MO, USA). Photoacid generator (PAG) was purchased from Craig Adhesive and Coating Co. (Newark, NJ, USA) under the compound name of UV9390C. It contains about 50 wt % of bis(4-dodecylphenyl)iodonium hexafluoroantimonate as an active ingredient. Synthesis of poly(phenyl-co-3-gylcidoxypropyl-co-perfluorooctyl)silsesquioxane (epoxy-SSQ) was done by a modified method that has been reported [18]. PTMS, FTES, and GTMS were used to synthesize Epoxy-SSQ. Mold release agent 1H,1H,2H,2H-perfluorodecyltrichlorosilane (FDTS) was purchased from Gelest Inc. (Morrisville, PA, USA). Silquest A-187 Silane (GTMS as the main ingredient) was purchased from Crompton Co. (Lisle, IL, USA). PET film was obtained from 3M Co. (St. Paul, MN, USA) with a thickness of 50 μm.

3.2.2. Instruments

A Nanonex 2000 imprinting tool (Monmouth Junction, NJ, USA) with vacuum capability and wavelength for UV curing at 365 nm or a light curing system (ELC-430) from Electro-Lite Corporation (Bethel, Ct, USA) is used for UV-NIL. Aluminum was deposited by electron-beam evaporation. Reactive ion etching (RIE) was conducted in a LAM 9400 tool (LAM Research Corporation, Fremont, CA, USA). Scanning electron microscopy (SEM) was performed by using a Hitachi SU8000 scanning electron microscope (Tokyo, Japan). Transmission of TM and TE was measured by using a HR4000CG spectrometer (Ocean Optics Inc., Dunedin, FL, USA) and a Nikon Eclipse TE300 microscope (Tokyo, Japan), with the assistance of high quality polarizer.

3.2.3. Nanoimprint process

The formulation of the nanoimprint resist is prepared by dissolving the epoxy-SSQ resin in PGMA, followed by the addition of PAG (1 wt % of the epoxy-SSQ resin). Original silicon oxide master molds are vapor-coated with FDTS in order to achieve easy mold release after the NIL processes. The epoxy-SSQ resin solution was spun on a flexible PET film substrate. The substrates were previously surface treated with O_2 plasma and then vapor coated with Silquest A-187 silane as an adhesion promoter to the SSQ resist material. The imprinting process is performed under UV light exposure for a few seconds at room temperature. A Nanonex 2000 imprinting tool with vacuum capability for UV curing at 365 nm or the light curing system (ELC-430) from Electro-Lite Corporation is used for imprinting and curing. The imprinting pressure is typically 40 psi.

3.2.4. Aluminum deposition

The rate of aluminum deposition in this study is 0.5 nm/s. In order to deposit aluminum on the sidewalls of the imprinted nanopattern but not on the base of the trench, the deposition mount is tilted to 40 degrees. The deposition process is repeated at the opposite direction to make aluminum deposition on both sidewalls of the SSQ nanogratings. This process is explained in Figure 3.1.

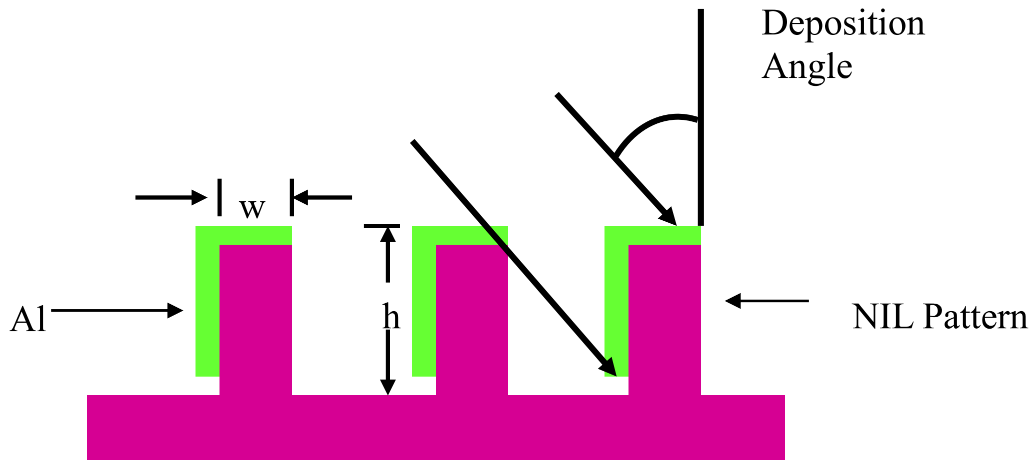

Figure 3.1. Angled deposition of aluminum on a nanopattern.

3.2.5. Plasma Ion etching process

For good polarizer performance, the aluminum layer deposited on top of the SSQ grating needs to be removed. We used an anisotropic plasma etching process to selectively remove the top aluminum while leaving the aluminum on the sidewall of the grating relatively intact. Aluminum etching was performed in the LAM 9400 tool. Aluminum etching had to be conducted in two steps under 200 W Transformer Coupled Plasma RF power. First, any residual aluminum oxide layer (thickness ~ 1 nm) was etched by using BCl_3 plasma (40 sccm) for 5 s, followed by the aluminum layer etching by using BCl_3 (20 sccm)/Cl_2 (6 sccm) plasma. The overall fabrication process of the WGP is illustrated in Figure 3.2.

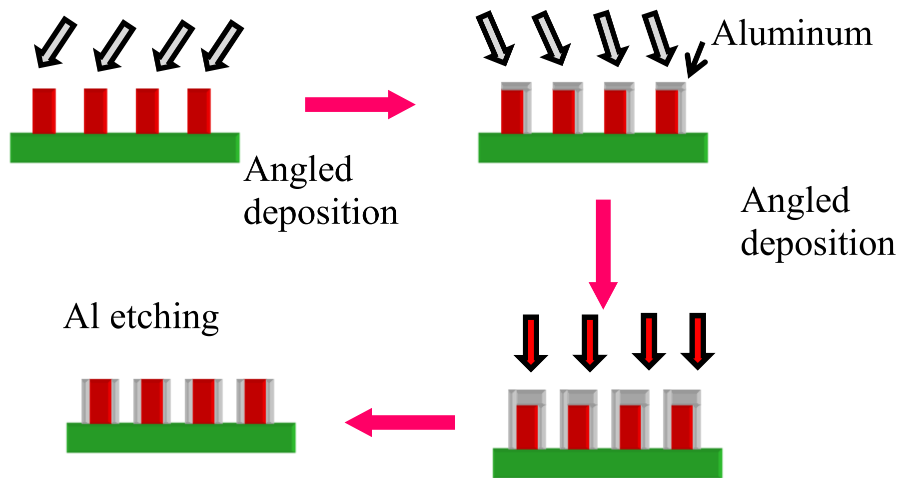

Figure 3.2. The total process involved in the fabrication of WGP in this study.

3.3. Results and discussion

3.3.1. Design consideration of the WGP

The purpose of this study is to fabricate a WGP which shows good performance across a wide wavelength range of the visible light by using NIL. It is well known that typical WGPs have a period lower than 150 nm in order to be used in the visible light range, as was done in previous WGPs fabricated using NIL. However it is challenging to fabricate molds with smaller periods and imprint with high yields, to relax the fabrication challenges, a method to create efficient WGPs by using molds with larger periods is desirable.

Our new method to fabricate WGPs used angled aluminum depositions on the nanoimprinted pattern from both the sides at a 40 degree angle from the normal direction. As shown in Figure 3.2, aluminum from the upper part of the pattern was removed by reactive ion etching. The final structure of the WGP has aluminum coatings on both sides of the nanoimprinted grating walls. A nanoimprinted pattern with a 220 nm period and a 70 nm linewidth was prepared by using NIL in this study to leave room for the aluminum coatings.

We carried out a simulation of the performance of the WGP by using COMSOL program to design the structure and optimize its polarization performance. The performance of the WGP is characterized by the high TM transmittance the high extinction ratio, defined as the ratio of transmittance of the TM polarized light to that of the TE polarized light. Fixing the period at 220 nm, linewidth at 70 nm, and sidewall Al coating at 30 nm, TM/TE transmission simulation results for heights varying from 100 nm to 250 nm are shown in Figure 3.3. Dips in the transmission curve are the result of Fabry-Perot resonances formed within the metallic nanoslits. The WGP with a 200

nm height showed a relatively flat TM transmission over the visible region as compared with the others.

We also simulated the performance of the WGP by changing the thickness of the aluminum deposition from 15 nm to 35 nm thick. The simulation results of TM values and TE values at the different wavelength for the WGPs are shown in Table 3.1. And the simulation results in the whole wavelength range of the visible light for WGPs with 30 nm or 20 nm aluminum deposition on the sidewalls were shown in Figure 3. 3.

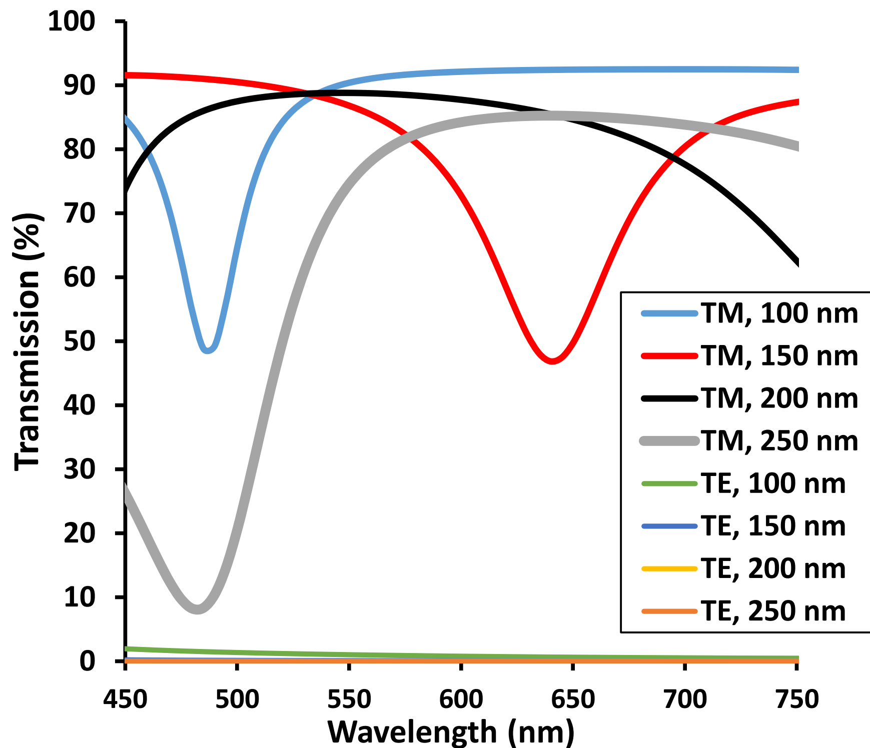

Figure 3. 3. Simulation results for the WGPs that contain the different heights of the nanopattern (220 nm period, 70 nm linewidth, 30 nm thickness of aluminum).

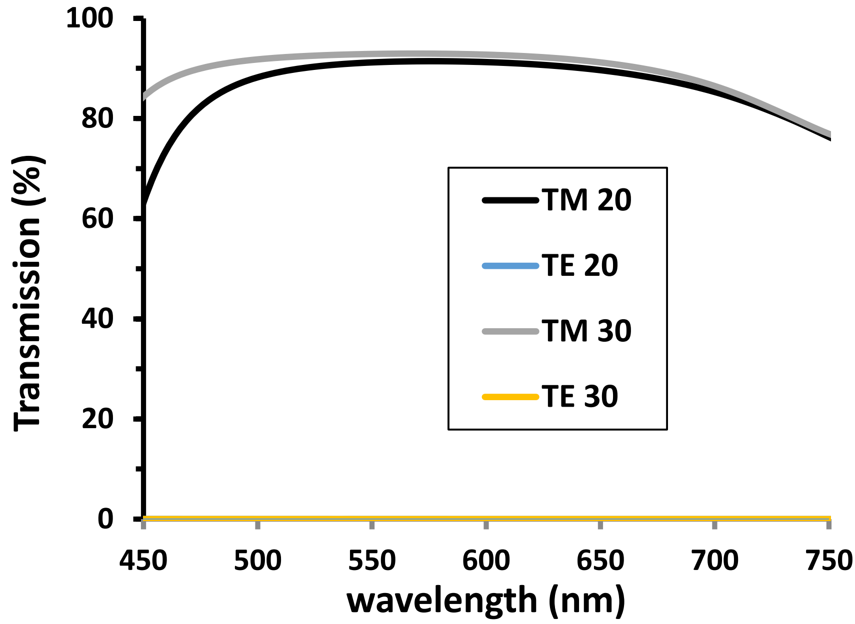

Figure 3. 4. Simulation results for WGPs that contain Epoxy-SSQ nanopattern with 20 nm and 30 nm aluminum deposition on both the sidewalls.

Table 3. 1. Simulation results of transmission (%) of TM/TE polarized light at the different wavelength for the WGPs for different thickness of aluminum deposition

Thickness (nm)	450 nm	550 nm	650 nm	750nm
15	47.4/0.789	91.8/0.268	91.9/0.131	83.6/0.0875
20	72.6/0.0267	89.5/0.00853	84.9/0.00414	68.1/0.00311
25	69.9/0.0678	90.0/0.244	87.2/0.0123	69.5/0.00835
30	78.6/0.00423	85.7/0.00118	79.5/0.000507	62.3/0.000354
35	74.3/0.00869	87.1/0.00299	81.7/0.00149	56.4/0.00103

3.3.2. Synthesis of Epoxy-SSQ and NIL

Epoxy-SSQ was synthesized from PTMS, FTES, and GTMS. The PTMS component helps to increase the hardness of the synthesized SSQ polymer and FTES helps to improve the releasing property of the imprinted SSQ patterns from the mold. GTMS contains the epoxy functional group which can polymerize during NIL via cationic polymerization, and make it immune to the oxygen environment. Epoxy-SSQ was synthesized by using the method that was modified from a previously reported method [77] in our group. The epoxy functional group shows good mechanical properties after the completion of curing, and simultaneously shows good adhesion. This property plays an important role in a NIL process to help the adhesion of the imprinted material with the substrate. Better mold releasing is also very important to ensure defect-free patterning over a large area. This was achieved by increasing the amount of FTES in the resist formulation. The SEM of the formed SSQ nanograting pattern is shown in Figure 3.5(a), showing well defined high-aspect ratio and uniform nanopattern. Most notably a very regular and uniform pattern without any defects was obtained in large area, due to the increase in the amount of FTES in the resist formulation for ease demolding.

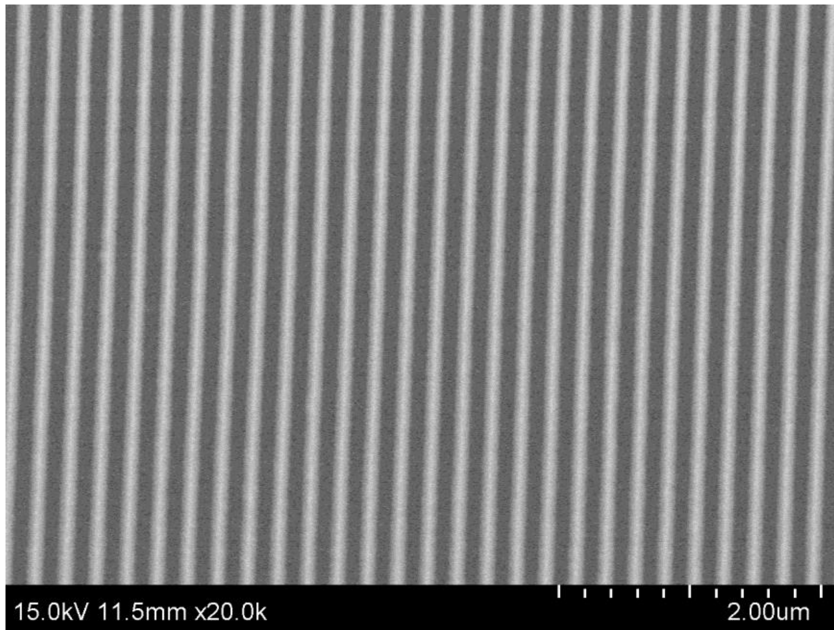

(a)

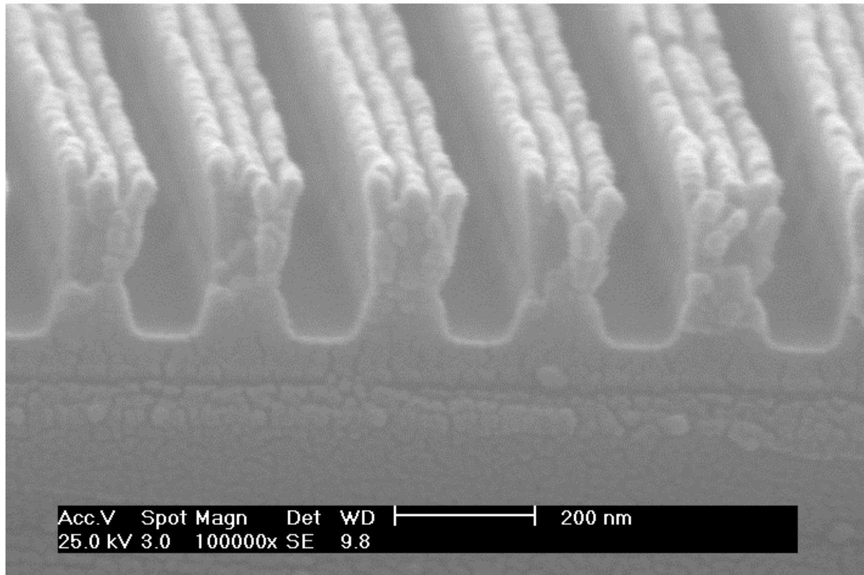

(b)

Figure 3. 5 SEM photograph of SSQ nano pattern on a flexible PET film (a) and the cross section of a nanopattern after aluminum deposition and ion etching (b).

3.3.3. Aluminum deposition and etching

In Figure 2, the structure of the obtained WGP was the aluminum coating at both the sides of the 70 nm nanopattern line. The SEM photograph of the fabricated WGP after aluminum deposition and etching is shown in Figure 3.5(b), where the aluminum layers at both side walls of the nanopatterns can be clearly seen. Note that this structure was damaged slightly by the reactive ion etching process.

As the WGP structure was fabricated on a PET film, the final WGP sheet is very flexible as the picture shown in Figure 3.6.

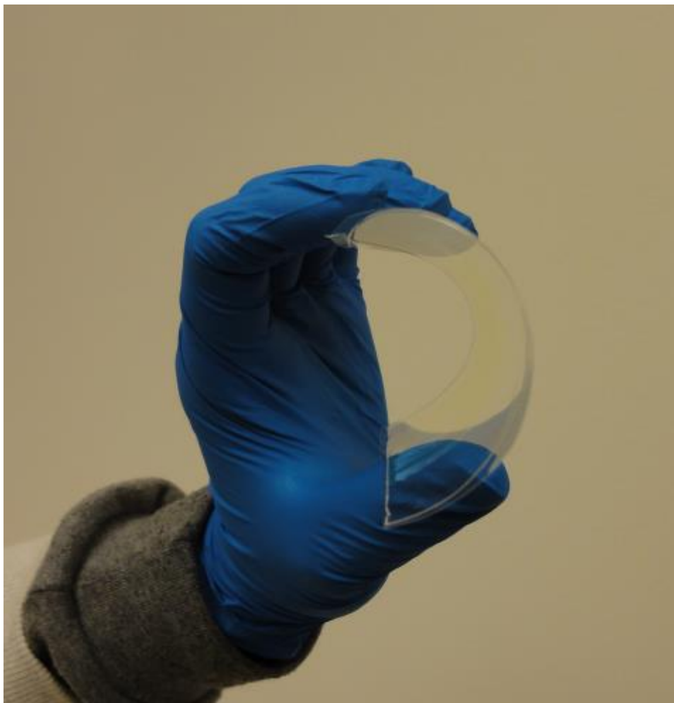

Figure 3.6. Flexibility of a PET film containing WGP structure.

3.3.4. Measurement of TM & TE transmission and extinction ratio

The optical property of the obtained WGP was estimated by measuring the transmittance of both the TM and the TE polarized-lights. The results of the measurement of TM and TE transmission for the fabricated WGPs are shown in Table 3.2. And the results in the whole wavelength range of the visible light for WGPs with 30 nm or 20 nm aluminum deposition on the sidewalls were shown in Figure 3.8.

Table 3.2. Measured optical transmission (%) of TM/TE polarized light through nanopatterned Epoxy-SSQ/aluminum WGPs at the different wavelength for the WGPs of different thickness of aluminum deposition on the SSQ grating sidewalls

Thickness (nm)	450 nm	550 nm	650 nm	750nm
15	50.6/6.53	90.3/0.670	89.7/0.179	82.1/9.43
20	70.5/4.65	85.8/0.082	90.6/0.031	82.9/9.09
25	71.1/5.09	89.5/0.097	81.7/0.104	75.9/11.3
30	77.7/5.02	80.3/0.100	82.4/0.039	74.7/10.4
35	70.8/5.12	78.9/0,377	80.1/0.235	68.2/11.2

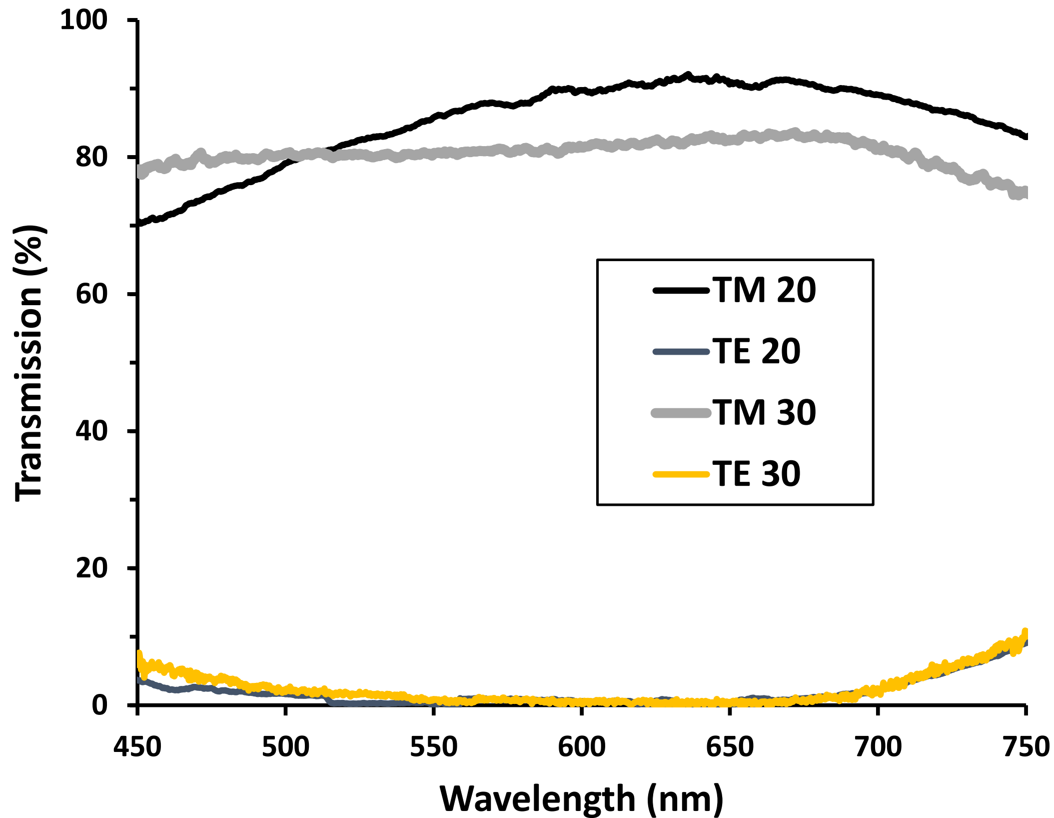

Figure 3.7. The TE & TM curves of a nanopatterned Epoxy-SSQ WGP with 20 nm and 30 nm aluminum deposition on both the sidewalls.

In the case of the WGP with 30 nm aluminum sidewall coatings, the result is shown in Figure 3.8., 75-85 % of the TM polarized-light was transmitted in the wide wavelength range of the visible light. On the other hand, below 5 % of the TE polarized-light was transmitted in the same wavelength range. And in case of the WGP with 20 nm aluminum coating, the result is shown in Figure 3.7, 70-90 % of the TM polarized-light was transmitted in the wide wavelength range of the visible light.

The extinction ratio (ratio of TM to TE) for the 30 nm coated WGP showed values of 803 at 550 nm, and 2117 at 650 nm while the 20 nm coated WGP showed ratios of 1046 at 550 nm, and 2900

at 650 nm. The TM transmission in Figure 3.7 showed the more flat curve in the wide wavelength range of the visible light.

3.4. Conclusion

Nanopatterns of 220 nm period, 70 nm linewidth, and 200 nm height were formed using synthesized Epoxy-SSQ on a flexible PET film. Angled aluminum depositions were performed at a 40 degree angle from the perpendicular plane and aluminum was removed from the top of the pattern by reactive ion etching. The obtained WGP had a unique structure in which aluminum coatings were on both the sides of the wall of the nanopattern. Despite using a larger period than previously reported WGPs, high extinction ratios were achieved over the visible spectrum with a simple fabrication process. If these results can be migrated to roll-to-roll processing methods [2, 3], efficient WGPs could be easily manufactured over large areas.

Chapter 4

Fabrication and Encapsulation of a Short-Period Wire Grid Polarizer with Increased Viewing Angle by the Angled-evaporation Method

4.1. Introduction

The liquid crystal display (LCD) is currently the prevailing display technology. An LCD requires polarized illumination to function [11, 62]. Therefore, polarizers are a very important part of an LCD and are also essential components in many optical systems and networks. The optical performance of conventional polarizers based on dichroic absorption cannot meet the requirements of some new optoelectronic systems currently under development. A wire grid polarizer (WGP) is one of the most attractive alternatives. The WGP is made of parallel metallic lines on a transparent substrate and is used to transmit transverse magnetic (TM) polarized light (E-field perpendicular to the grating) and reflect transverse electric (TE) polarized light (E-field parallel to the grating direction).

WGPs offer a large spectral range and small size, and they can be integrated with other optical elements on the same chip. They can also be constructed as high-quality, integration-capable, thin-film-type polarizers[1, 32, 55, 71, 72, 95-97]. WGPs can be applied to various fields such as microscopy, imaging systems, and polarized beam splitters. WGPs in the visible optical region were reported a decade ago by the MOXTEK group as beam splitters for projection displays[28, 39]. WGPs may improve the brightness of LCDs because their function is not based on light absorption, and reflected light can be recycled[100]. However, for direct-view liquid crystal displays, a WGP can only be used as a bottom polarizer but cannot replace the top dichroic polarizers, because it would reflect ambient light[30]. One potential solution was developed by adding an absorptive interference layer on top of the Al grating to reduce light reflection [89]. Still much investigation in both design and fabrication are needed to push the WGP to practical application. Additionally, displays for mobile devices have progressed toward increasingly thinner, lighter, and more flexible devices. Future flexible displays could benefit from the WGPs made on a polymer substrate.

TM transmission and TE suppression are the most important features of WGPs, and hence the extinction ratio, which is defined as the ratio of TM transmission to the TE transmission, is also an important factor. The optical properties of a WGP are determined by the grating material, the period and line width of the grating, and the grating height[40]. In the last two decades, various research results on the fabrication of WGPs using nanoimprint lithography (NIL) have been reported[1, 32, 55, 71, 72, 95-97]. For example, a bilayer metal WGP was presented by Ekinci et al.[24]. The fabrication of a flexible nano-wired polarizer by contact-transferred and mask-embedded lithography using a polyurethane acrylate mold was described by Hsu et al. [41]. NIL has been used in recent years due to its potential for high resolution and high throughput nanoscale

patterning to produce the fine pitch required for a WGP[4, 13, 15-17, 36]. We also reported previously the fabrication of bilayer metal WGPs on flexible plastic substrates by roll-to-roll UV nanoimprint lithography and the metal evaporation technique[15], and a WGP embedded in gas-permeable membrane for contact lens application[40]. Particularly, the high throughput UV-NIL process has the potential to enable large area metal WGP fabrication[2, 3].

WGPs require fabrication of subwavelength metal gratings, which presents a significant challenge for patterning and etching of dense structures, particularly for use in visible-wavelength applications. It becomes even more challenging to fabricate these structures on a flexible substrate. It is known that the WGP should have a period shorter than 150 nm in order to provide adequate bandwidth to cover the visible light range. In our previous publication[86], a flexible WGP was fabricated on a polyethylene terephthalate (PET) film with an imprinted 220 nm-period high-aspect-ratio polymer grating with double-angled aluminum deposition to cover the sidewalls of the imprinted polymer grating. Isotropic reactive ion etching (RIE) was then used to remove selectively the aluminum deposited on the top of the grating, thereby forming metal wire grids with spacing much closer than lithographically defined gratings. Even though the imprinted grating had a relatively large period of 220 nm, the obtained WGP showed good performance in the wide visible band of the spectrum due to a much narrower spacing between the aluminum lines. As a result, good optical performance was obtained in the visible band of the spectrum. This approach significantly relaxes the stringent requirement for the fine line patterning process used in traditional methods, and is particularly desirable for future manufacturing of flexible WGPs using the roll-to-roll nanoimprint process. For practical application, encapsulation of the WGP is highly desirable to improve the mechanical integrity of the high aspect ratio metallic nanogratings and makes it easier to integrate with other optical components. The polarizer performance degrades

when light is incident from a higher angle. This study shows that these issues can be addressed by reducing the period of the grating. In particular we fabricated the WGP using a grating mold with a 180 nm period to prove the principle.

4.2. Experimental

4.2.1. Materials and the Synthesis of Imprinting Material

Phenyltrimethoxysilane (PTMS), (3-glycidyloxypropyl)trimethoxysilane (GTMS), (tridecafluoro-1-octyl)triethoxysilane (FTES), CsOH, and propylene glycol monomethyl ether acetate (PGMA) were purchased from Aldrich Chemical (St. Louis, MO, USA). Photoacid generator (PAG) was purchased from Craig Adhesive and Coating Co. (Newark, NJ, USA) under the compound name of UV9390C. It contained ~50 wt% of bis(4-dodecylphenyl)iodonium hexafluoroantimonate as an active ingredient. Synthesis of poly(phenyl-co-3-gylcidoxypropyl-co-perfluorooctyl)silsesquioxane (epoxy-SSQ) was carried out by a previously reported method [20,21]. PTMS, FTES, and GTMS were used to synthesize epoxy-SSQ. The mold release agent 1H,1H,2H,2H-perfluorodecyltrichlorosilane (FDTS) was purchased from Gelest, Inc. (Morrisville, PA, USA). Silquest A-187 silane (GTMS as the main ingredient) was purchased from Crompton Co. (Lisle, IL, USA). PET film with a thickness of 50 μm was obtained from 3M Co. (St Paul, MN, USA). PMMA (average M_w 120,000) for encapsulation was purchased from Aldrich.

4.2.2. Instruments

A Nanonex 2000 imprinting tool (Monmouth Junction, NJ, USA) with vacuum capability and UV curing at 365 nm, or a visible light curing system (ELC-430) from Electro-Lite Corporation (Bethel, CT, USA) was used for UV-NIL. Aluminum was deposited by electron-beam evaporation. RIE was conducted in a Lam 9400 TCP Poly Etcher tool (Lam Research Corporation, Fremont, CA, USA). Scanning electron microscopy was performed using a Hitachi SU8000 SEM (Tokyo, Japan). Transmission of TM and TE energy was measured using an HR4000CG spectrometer (Ocean Optics, Inc., Dunedin, FL, USA) and a Nikon Eclipse TE300 microscope (Tokyo, Japan) with the assistance of a high-quality polarizer. In order to measure the viewing angle, the sample was mounted so it could be tilted to the desired angle. The simulation was performed using the COMSOL program, and by the rigorous coupled wave analysis (RCWA) method. An ellipsometer (AutoEL) was used to measure the refractive index and the thickness of the thin films.

4.2.3. Nanoimprint Process

The formulation of the nanoimprint resist was prepared by dissolving epoxy-SSQ resin in PGMA, followed by the addition of PAG (1 wt% of the epoxy-SSQ resin). The original silicon oxide master molds were vapor coated with FDTS for easy mold release after the NIL processes. The epoxy-SSQ resin solution was spin coated onto a flexible PET film substrate. The substrates were first surface treated with O_2 plasma and then vapor coated with Silquest A-187 silane to promote adhesion to the SSQ resist material. The imprinting process was performed under UV light for a few seconds at room temperature. The Nanonex 2000 imprinting tool or the ELC-430

light curing system was used for imprinting and curing. The imprinting pressure was typically 275 kPa.

4.2.4. Aluminum Deposition

The rate of aluminum deposition in this study was 0.5 nm/s. In order to deposit aluminum on the sidewalls of the imprinted nanopattern but not on the base of the trench, the deposition mount was tilted at 40º. The deposition process was repeated in the opposite direction to deposit aluminum on both sidewalls of the SSQ nanogratings. The thickness of aluminum on both sidewalls was controlled to be 20 nm. This process is illustrated in Figure 1.

4.2.5. Reactive Ion Etching Process

For good polarizer performance, the aluminum layer deposited on the top of the SSQ grating needed to be removed. We used an anisotropic plasma etching process to remove the top layer of aluminum selectively while leaving the aluminum on the sidewalls of the grating relatively intact. Aluminum etching was performed using the Lam 9400 tool. The aluminum etching had to be conducted in two steps under 200 W of transformer-coupled plasma RF power. First, any residual aluminum oxide layer (thickness, ~1 nm) was etched with 40 sccm of BCl_3 plasma for 5 s, followed by etching the aluminum layer with 20 sccm BCl_3/6 sccm Cl_2 plasma.

4.2.6. Encapsulation of WGP

PMMA (0.50 g) was dissolved in 100 mL of acetone, and the fabricated WGP was dipped

in this solution. The fabricated WGP was removed from the PMMA solution and hung vertically for 15 min at room temperature. This encapsulated WGP was dried in an oven for 60 min at 60 ℃. The coating thickness was controlled to be less than 1 μm.

4.3. Results and Discussion

4.3.1. Simulation of Angle Dependency

The WGP which was reported in our previous paper[86] showed a large angle dependency and had a narrow viewing angle. Consequently, the TM transmission was reduced greatly even at a 30º incident angle. A wide viewing angle is an important requirement for display devices such as an LCD. In order to improve the angle dependency of the WGP, we first tried simulations with a shorter period WGP. A nanoimprinted pattern with a 180 nm period, 70 nm linewidth, and 200 nm height was used as a model system, and 20 nm aluminum gratings were deposited along both walls of the patterned grating lines. The final WGP had a structure with periodic 20 nm wide aluminum gratings with 70 nm spacing.

Figures 4.1 (a) and (b) show the simulation results of the angle dependency for the WGPs made from the polymer gratings with initial periods of 220 and 180 nm, respectively. The simulation was conducted using the refractive index data of the base materials. The refractive index was measured by an ellipsometer (AutoEL), and the coating thickness was also measured.

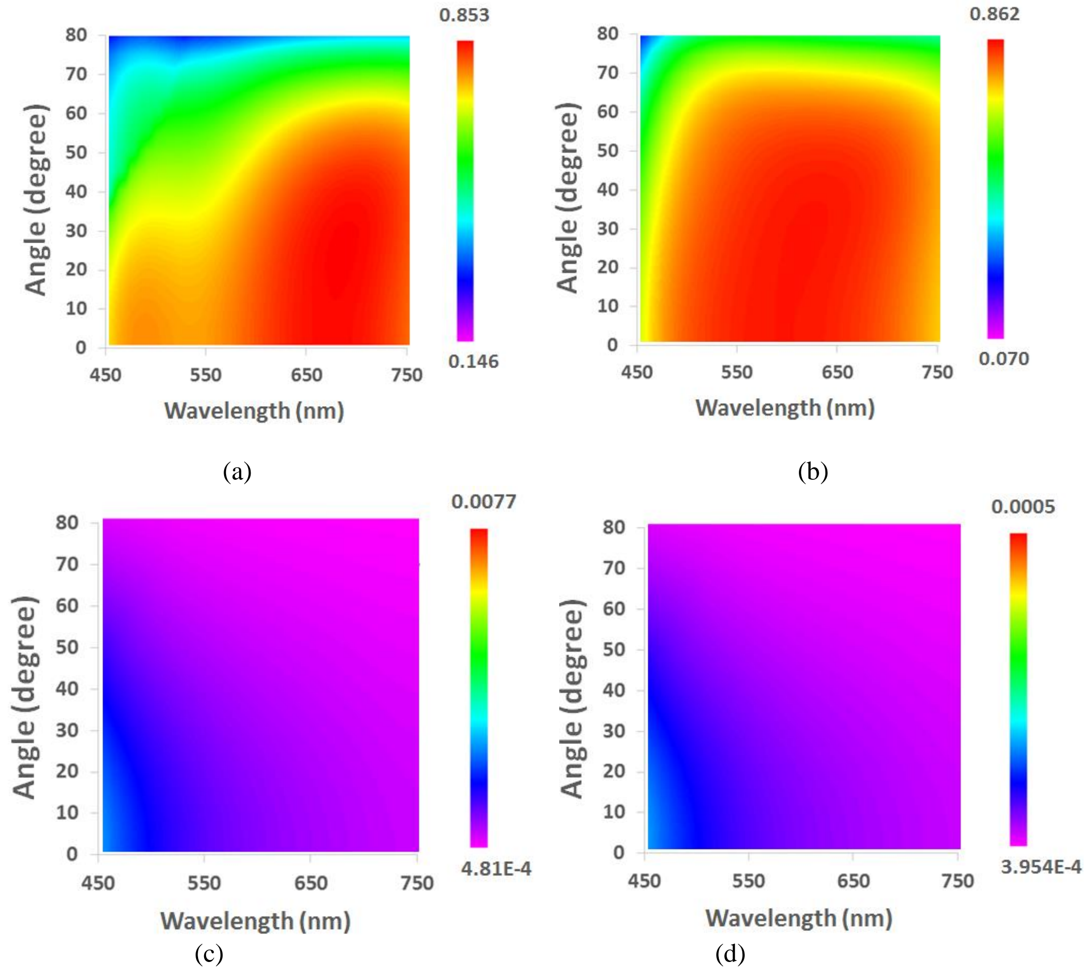

Figure 4.1. Simulation results showing the angle dependency for WGPs of 220 nm-period polymer grating [TM transmission (a) and TE transmission (c)], and by a 180 nm-period polymer grating [TM transmission (b) and TE transmission (d)]. The height of the nanograting is 200 nm, and the thickness of the aluminum coating on the grating sidewall is 20 nm.

In Figures 4.1(a) and (b), the red-colored region indicates a high transmission of TM light, and the purple indicates low transmission of TM light. Improved angular performance is obvious for the shorter period grating. For example, at 500 nm, the transmission of the TM light improved greatly for the WGP with a 180 nm period at incident angles greater than 30º. The overall angle dependency of the WGP with a 180 nm period was better than that of the WGP with a 220 nm

period at visible wavelengths. In Figures 1(c) and (d) the transmission levels of TE light are both below 0.008 and showed a similar pattern. Therefore the extinction ratio of the WGP also improves at a large viewing angle for shorter-period gratings[96].

4.3.2. Fabrication of the WGP

An effective method for fabricating WGPs with shorter periods is to use double-angled aluminum depositions onto both sides of the nanoimprinted polymer grating walls[86]. The aluminum at the upper part of the pattern can be removed by RIE. This process is shown in Figure 4.2. The final structure of the WGP has aluminum coatings on both sides of the nanoimprinted grating walls. A nanoimprinted pattern with a 180 nm period, 70 nm linewidth, and 200 nm height was prepared using NIL in this study to ensure adequate allowance for the aluminum coatings. Therefore, the final structure of the WGP after completing the entire process had a periodic 70 nm linewidth, 20 nm aluminum grating, 70 nm interval, and 20 nm aluminum grating, as shown in Figure 2. The overall fabrication process of the WGP is illustrated in Figure 4.2.

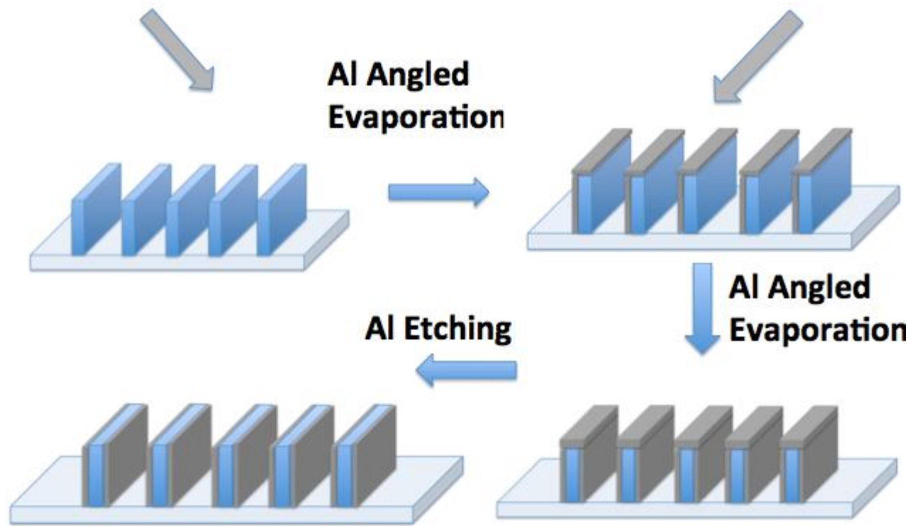

Figure 4.2. Double-angled evaporation of aluminum onto a nanopattern and the reactive ion etching process.

To imprint the polymer grating, we used silsesquioxane (SSQ) resist materials that were reported previously[76, 77]. Briefly, poly(phenyl-co-3-gylcidoxypropyl-co-perfluorooctyl)silsesquioxane (epoxy-SSQ) was synthesized from phenyltrimethoxysilane (PTMS), (tridecafluoro-1-octyl)triethoxysilane (FTES), and (3-glycidy¬loxy¬propyl)trimethoxysilane (GTMS). The PTMS component helps to increase the hardness of the synthesized SSQ polymer, and FTES helps to improve the releasing property of the imprinted SSQ patterns from the mold. GTMS contains an epoxy functional group which can polymerize during NIL via cationic polymerization. The epoxy functional group shows good mechanical properties after the completion of curing and simultaneously shows good adhesion [76, 77, 86]. This property plays an important role in the NIL process to increase the adhesion of the imprinted material to the substrate, particularly for a dense, narrow linewidth and the high aspect ratio features required for a WGP. Better mold releasing is

also very important to ensure defect-free patterning over a large area. Figure 4.3 (a) is a scanning electron microscope (SEM) image of the formed SSQ nanograting pattern showing a well-defined and uniform high aspect ratio nanopattern with a 70-nm linewidth and 180 nm period. The SEM image of the fabricated WGP after double side angled aluminum depositions at 40 degrees and after RIE are shown in Figures 4.3 (b) and (c), respectively, where the aluminum layers on both side walls of the nanopatterns can be clearly seen.

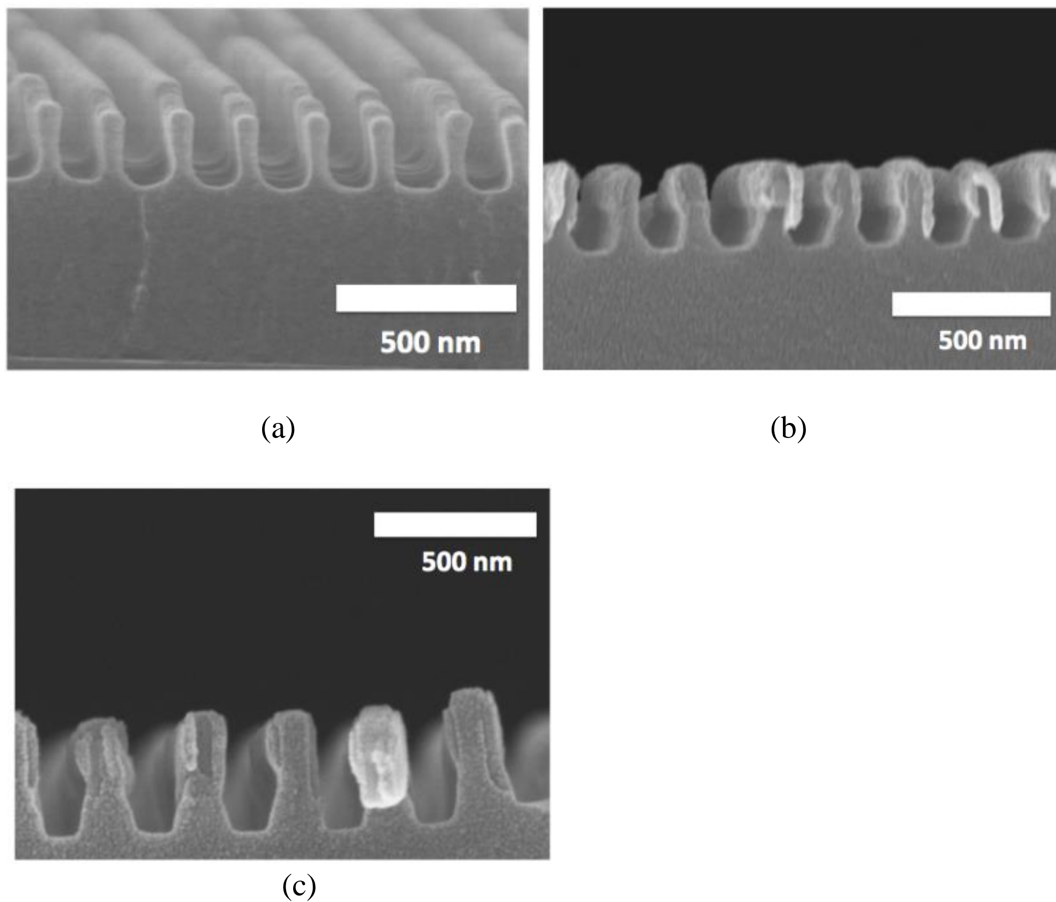

Figure 4.3. (a) SEM image of an SSQ nanopattern on a flexible PET film, and the cross section of a nanopattern (b) after aluminum deposition and (c) after RIE.

4.3.3. Optical Properties of the WGP

The optical properties of the obtained WGP were characterized by measuring the transmittance of both the TM and the TE of polarized light. The results of the measurement of TM and TE transmission for the fabricated WGPs are listed in Table 4.1, in the visible range for the WGPs shown in Figure 4.3. In Figure 4.4, 80–90% of the TM polarized light was transmitted in the wide visible wavelength range of 450–700 nm. Only 0.5–2% of the TE polarized light was transmitted in the same wavelength range.

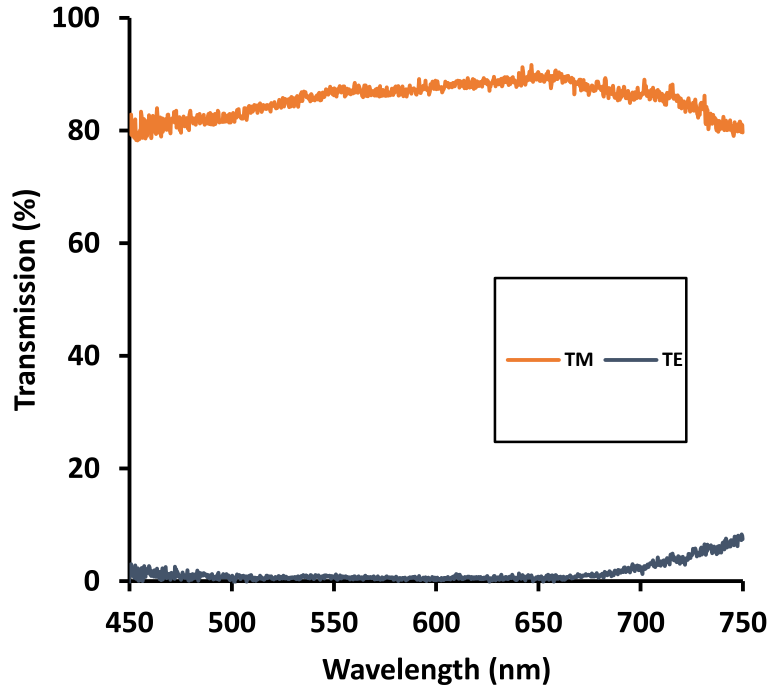

Figure 4.4. The TE and TM curves of a nanopatterned epoxy-SSQ WGP with 20 nm aluminum deposition on both sidewalls (180 nm period, 70 nm linewidth, 200 nm grating height).

Table 4.1. Measured optical transmission (%) of TM/TE polarized light through nanopatterned epoxy-SSQ/aluminum WGPs.

	450 nm	550 nm	650 nm	750 nm
TM/TE	79.4/1.03	83.1/0.74	88.4/0.67	79.7/7.47

The angle dependencies of the 220 and 180 nm period WGPs were measured. The data are shown in Figure 4.5.

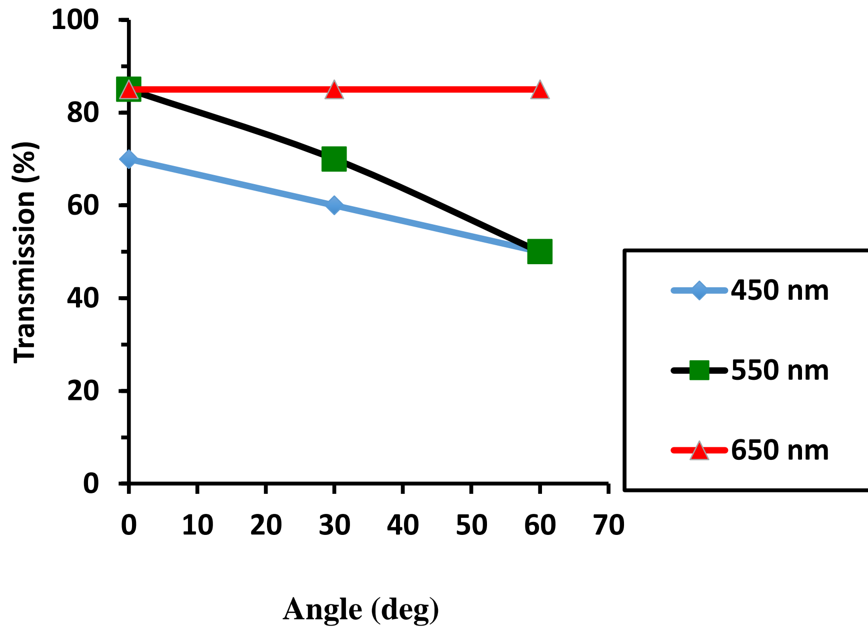

(a)

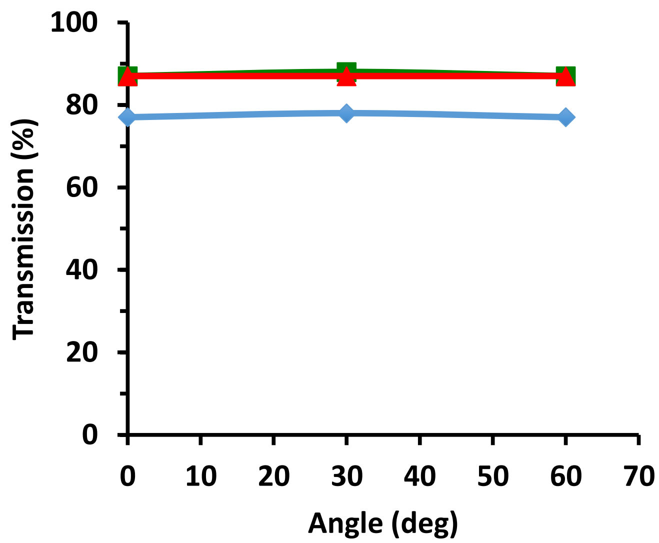

(b)

Figure 4.5. The transmission of TM light for (a) the 220-nm period WGP and (b) the 180-nm period WGP.

In the case of the WGP fabricated from the imprinted 220 nm period grating, the transmission of TM light was reduced abruptly for 450 nm wavelength light as the angle was increased to 60º. The reduction was more gradual at 550 nm as the angle was increased to 60º. Further, no significant reduction was observed at 650 nm. In comparison, for the WGP fabricated from the 180 nm period grating, the transmission of TM light was not reduced at any visible wavelength as the angle was increased to 60º.

Finally, we would like to discuss the optical performance of the WGP after the fabricated Al nanogratings are embedded in a polymer layer for protection. Such encapsulation of the WGP is very important for practical use; however, the encapsulating material must have minimal effect on the optical property of the WGP. A simulation was conducted for a WGP structure with a 90 nm period, 20nm wide Al grating and, 200 nm height after encapsulation by materials with refractive indexes of 1.0 (e.g. air), 1.5 (typical polymer), and 2.0 (high index material). The results are shown in Figure 4.6.

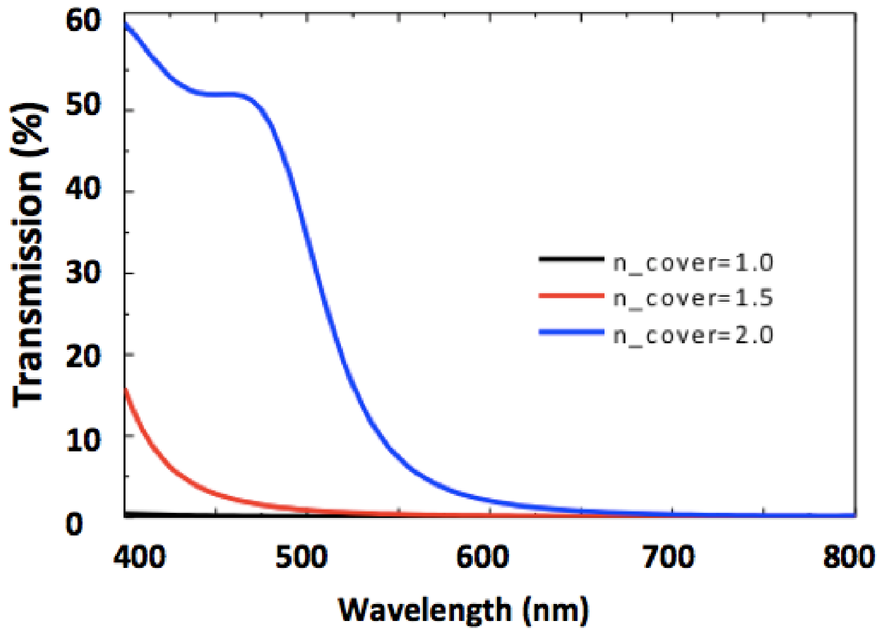

Figure 4.6. The simulation data for the refractive index of the encapsulating material affects the TE transmission. Refractive indexes are black 1.0, red 1.5, and blue 2.0.

The results showed that when the refractive index of the encapsulating material is 2.0, the TE transmission is not blocked. This means that material like this cannot be used for encapsulation of a WGP. However, when the refractive index of the encapsulating material is 1.5, there is no problem in using it for the encapsulation of a WGP. Therefore, we chose PMMA as the encapsulating material for the WGP because the refractive index of PMMA is 1.49.

Encapsulation of the WGP with PMMA was conducted by the dip-coating method. The coating thickness was controlled to be less than 1 μm. A simulation was conducted to estimate the effect of the coating thickness on TM and TE. The results are shown in the supporting information. The transmission of TE and TM light were then measured for the encapsulated WGP. The result is shown in Figure 4.7.

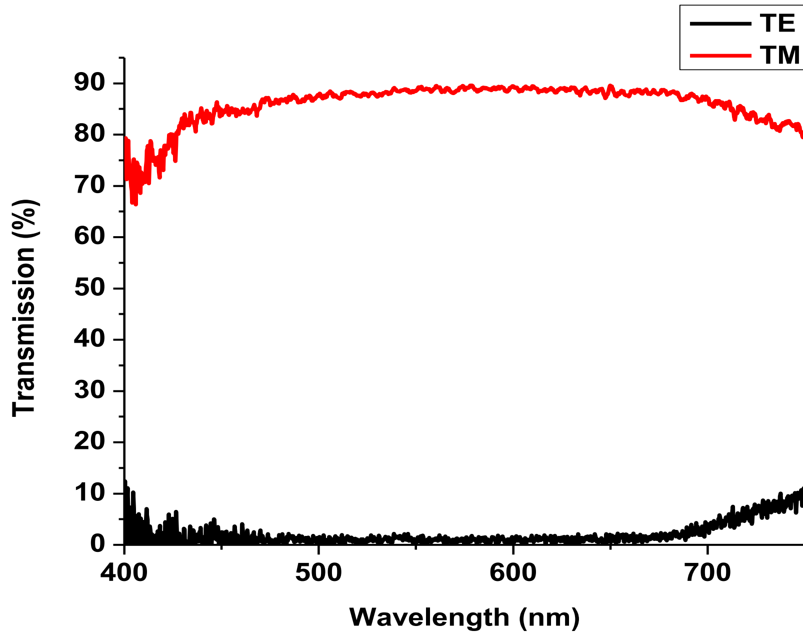

Figure 4.7. The TE and TM curves of a nanopatterned epoxy-SSQ WGP after PMMA encapsulation.

Nearly all of the data plotted in Figure 4.7 are similar to the data plotted in Figure 4.3. This implies that the encapsulation of the WGP in PMMA does not affect the performance of the WGP.

4.3.4. Measurement of the refractive index and thickness of the polymerized epoxy-SSQ

An ellipsometer (AutoEL) was used to measure the refractive index and the thickness of thin films. Silicon was used as a substrate, and epoxy-SSQ was spin-coated onto this substrate. After UV curing, the refractive index and the thickness were measured. The thickness of the coating was controlled to be 200 nm.

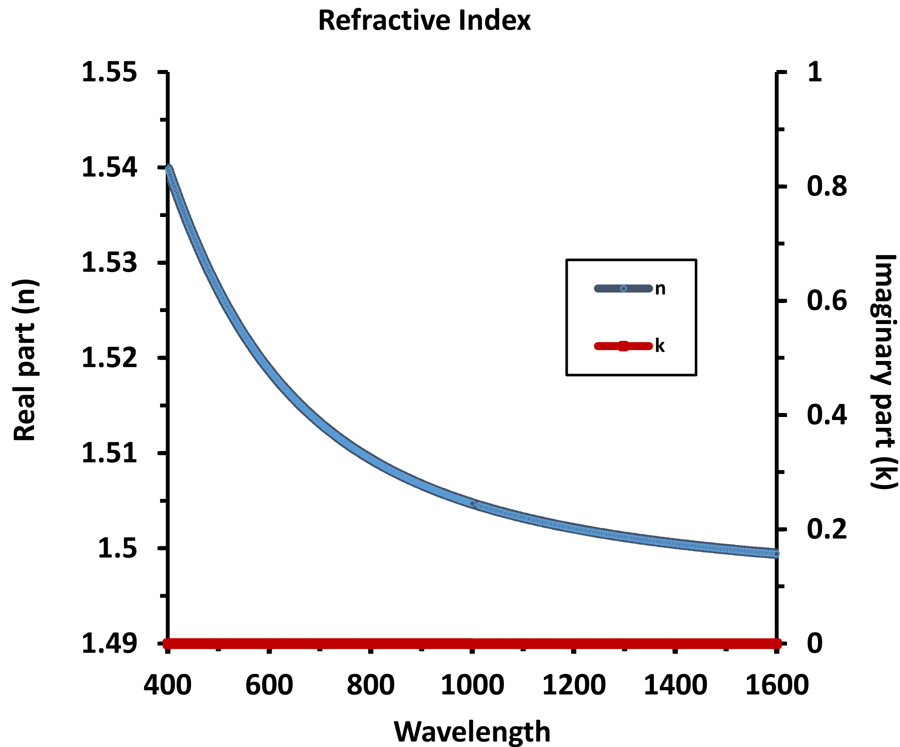

Figure 4.8. The refractive index of the polymerized epoxy-SSQ measured with an ellipsometer.

This refractive index data was used for angle simulation and encapsulation simulation. The refractive index of the general polymer is known to be ~1.5 in the visible wavelength range. The refractive index consists of 2 parts: *n* is a real part of the refractive index, which indicates the phase speed, while *k* is the imaginary part, which indicates the amount of absorption loss when the electromagnetic wave propagates through the material. This result shows that *k* is nearly 0 in the visible wavelength range.

4.3.5. Simulation results for the effect of the coating thickness on TM and TE

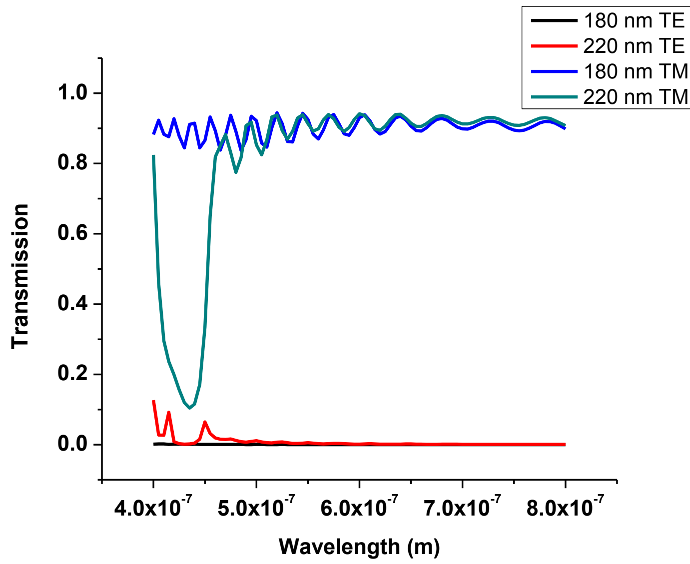

Figure 4.9. Simulations of TM and TE with 4 μm encapsulation of PMMA.

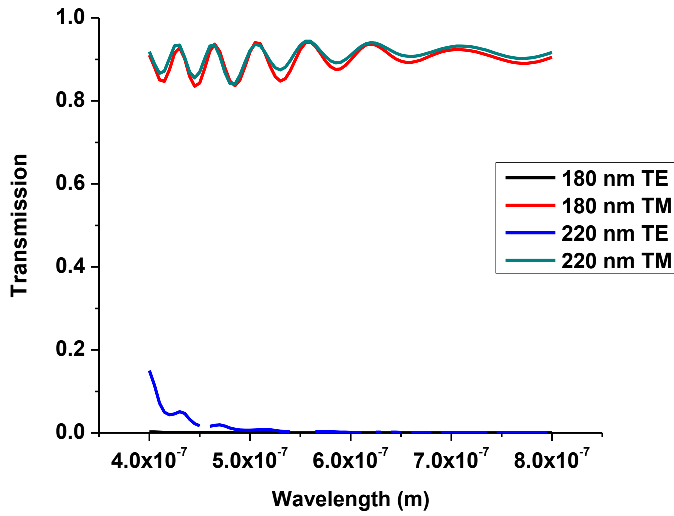

Figure 4.10. Simulations of TM and TE with 2 μm encapsulation of PMMA.

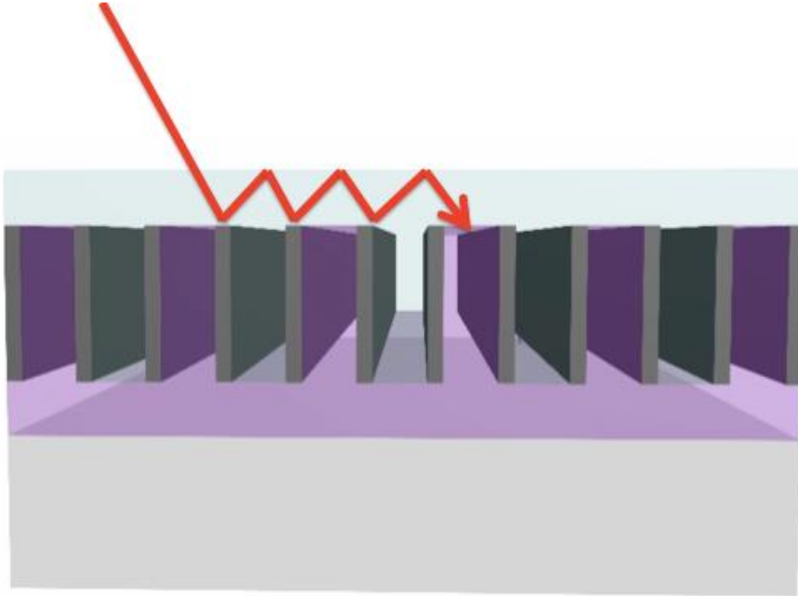

Figure 4.11. Fabry–Perot resonance [82, 94] between aluminum gratings and PMMA.

A simulation was conducted to estimate the effect of the coating thickness on TM and TE. The results are shown in Figures 4.9 and 4.10. In the case of a 4 μm coating thickness and 220 nm grating, the TM values dropped between 410 nm and 450 nm. The oscillatory behavior is shown in Figures 4.2 and 4.3. These phenomena were induced from the Fabry-Perot resonance, which is shown in Figure 4.4. Such resonance can be suppressed by using thinner overcoating. Therefore the encapsulation should be thin enough. Resonance effect can be observed for the 220 nm period embedded structure and cannot be used as a polarizer in the blue wavelength range. However, such effect is suppressed in the shorter period grating of 180nm.

4.4. Conclusion

In the present study, a WGP was fabricated by nanoimprint lithography, double-side angled evaporation of aluminum, and anisotropic RIE to remove the aluminum deposited on the top of the grating. The final structure of the Al grating has a 90 nm period, and about 20 nm aluminum linewidth. This WGP showed good performance in a wide range of visible wavelengths, which is not affected much at increased viewing angle. The WGP can be encapsulated in PMMA for practical use.

Chapter 5

Concluding Remarks

5.1. Contribution of nanoimprint materials

I developed a Young's-modulus-tunable epoxy resin and used it with nanoimprint lithography to increase the Young's modulus and decrease the brittleness of cured nanoimprint resists. The rigiflex [88] materials for nanoimprint lithography should show appropriate Young's moduli so that cured rigiflex materials are flexible enough to permit fine nanopatterning [83]. The epoxy resin was formulated using bisphenol F-type and NBR-based epoxy resins. The Young's modulus was tuned simply by changing the ratio of the two epoxy resins in the mixture. Adding NBR-modified epoxy resin greatly increased the impact strength of the mixed resin, which enabled higher-aspect-ratio structures to be fabricated using nanoimprint lithography.

And atomic layer deposition could be used to deposit two consecutive nanoimprinted layers in order to fabricate ultrasmall, high-aspect-ratio nanostructures.

5.2. Contribution of mold fabrication

Using electron beam lithography, the method most commonly used for nanofabrication, to fabricate sub-20-nm nanostructures remains very challenging and very expensive [18, 33, 53]. I used atomic layer deposition to economically fabricate ultrasmall nanostructures. A nanopattern showing a 60-nm-deep trench was obtained after the initial nanoimprinting; the trench depth was then reduced to 20 nm after the second nanoimprinting. The final pattern served as a mold to fabricate a 20-nm-deep, 9:1-aspect-ratio, ultrasmall nanostructure.

The residual layer in the nanopattern was removed using reactive-ion etching (RIE) with O_2 plasma. Further RIE could be used to remove the entire resist if a mistake had been made during nanoimprinting. SSQ shows considerable etching resistance, so RIE could not be used to remove SSQ resists. The silicon wafer was etched using RIE with HBr and He, and the remaining nanopattern was used as a mask. This method could also be used for molds larger than 2 in. × 2 in. In particular, our resist could be used for fabricating semiconductor processing materials. Furthermore, I developed a simple method of fabricating ultrasmall, high-aspect-ratio patterns.

5.3. Contribution of WGP fabrication method

The previously described nanopatterns can be applied in a number of research fields. I fabricated a WGP because it shows good polarization efficiency, long-term stability, a wide viewing angle, and the potential to be integrated with other optical components, unlike conventional polarizers. However, fabricating high-performance WGPs remains difficult because electron beam lithography is still commonly used to fabricate WGPs. We developed a more convenient method of fabricating such polarizers. I first used SSQ to synthesize a 220-nm-period, 70-nm-linewidth, 200-nm-high nanopattern on a flexible PET film and subsequently used it to fabricate a WGP. Two aluminum layers were deposited 40° from the perpendicular plane on both sides of the WGP, and RIE was subsequently used to remove the aluminum from the top of the pattern. The resulting WGP showed a unique structure in which both sides of the nanopattern wall were coated with aluminum. High extinction ratios were achieved over a wide range of visible wavelengths despite using a larger-period nanopattern and simple fabrication. Efficient WGPs could be easily manufactured using our method if these results can be extended to roll-to-roll processing.

5.3.1. Decreasing angular dependency of WGP

The polarizer viewing angle is one of the most important properties of optical components such as LCDs [26, 64, 65]. I used nanoimprint lithography and 180-nm-period, 70-nm-linewidth,

200-nm-high nanopatterns to fabricate a more efficient, wider-viewing-angle WGP. The angled aluminum layers on both sides of the WGP were subsequently evaporated, and anisotropic RIE was used to remove the aluminum layer deposited on top of the grating. Although 180-nm-period nanopatterns were used, the final aluminum grating showed a 90-nm period and ~20-nm aluminum linewidth. The wider-viewing-angle WGP exhibited good performance over a wide range of visible wavelengths. The viewing angle of this WGP was significantly wider than that of the previously obtained one.

5.3.2. Encapsulation of WGP

The WGP must be encapsulated for practical use; otherwise, the aluminum grating could be delaminated when the substrate is subjected to stress or could be damaged in harsh environments. Thus, I encapsulated the WGP in a <1-µm-thick PMMA layer. The encapsulated WGP showed good performance, almost the same as the unencapsulated WGP. In summary, I developed a very convenient method of fabricating a high-performance WGP. My method can be used to industrially mass-produce WGPs.

Reference

[1] Ahn S-W, Lee K-D, Kim J-S, Kim S H, Park J-D, Lee S-H and Yoon P-W 2005 Fabrication of a 50 nm half-pitch wire grid polarizer using nanoimprint lithography *Nanotechnology* **16** 1874

[2] Ahn S H and Guo L J 2008 High-Speed Roll-to-Roll Nanoimprint Lithography on Flexible Plastic Substrates *Advanced materials* **20** 2044-9

[3] Ahn S H and Guo L J 2009 Large-area roll-to-roll and roll-to-plate nanoimprint lithography: a step toward high-throughput application of continuous nanoimprinting *ACS nano* **3** 2304-10

[4] Ahn S H, Kim J-S and Guo L J 2007 Bilayer metal wire-grid polarizer fabricated by roll-to-roll nanoimprint lithography on flexible plastic substrate *Journal of Vacuum Science & Technology B: Microelectronics and Nanometer Structures* **25** 2388-91

[5] Alonso J M, Ondarçuhu T and Bittner A M 2013 Integration of plant viruses in electron beam lithography nanostructures *Nanotechnology* **24** 105305

[6] Arnold S, Gardner E, Hansen D and Perkins R 2001 52.3: An Improved Polarizing Beamsplitter LCOS Projection Display Based on Wire-Grid Polarizers(vol 32): Wiley Online Library) p 1282-5

[7] Back F, Bockmeyer M, Rudigier-Voigt E and Löbmann P 2013 Hybrid polymer sol–gel material for UV-nanoimprint: microstructure and thermal densification *Journal of Sol-Gel Science and Technology* 1-11

[8] Bailey T, Choi B, Colburn M, Meissl M, Shaya S, Ekerdt J, Sreenivasan S and Willson C 2000 Step and flash imprint lithography: Template surface treatment and defect analysis *Journal of Vacuum Science & Technology B: Microelectronics and Nanometer Structures* **18** 3572-7

[9] Bird G R and Parrish Jr M 1960 The wire grid as a near-infrared polarizer *JOSA* **50** 886

[10] Canalejas-Tejero V, Carrasco S, Navarro-Villoslada F, Fierro J L G, del Carmen Capel-Sánchez M, Moreno-Bondi M C and Barrios C A 2013 Ultrasensitive non-chemically amplified low-contrast negative electron beam lithography resist with dual-tone behaviour *Journal of Materials Chemistry C* **1** 1392-8

[11] Chen J, Kim K H, Jyu J J, Souk J, Kelly J and Bos P 1998 21.2: Optimum Film Compensation Modes for TN and VA LCDS(vol 29): Wiley Online Library) p 315-8

[12] Chen T K and Shy H J 1992 Effects of matrix ductility on rubber/matrix interfacially modified epoxy resins *Polymer* **33** 1656-63

[13] Cheng X, Guo L J and Fu P F 2005 Room-Temperature, Low-Pressure Nanoimprinting Based on Cationic Photopolymerization of Novel Epoxysilicone Monomers *Advanced Materials* **17** 1419-24

[14] Choi K M and Rogers J A 2003 A photocurable poly (dimethylsiloxane) chemistry designed for soft lithographic molding and printing in the nanometer regime *Journal of the American Chemical Society* **125** 4060-1

[15] Choi P, Fu P F and Guo L J 2007 Siloxane copolymers for nanoimprint lithography *Advanced Functional Materials* **17** 65-70

[16] Chou S Y, Krauss P R and Renstrom P J 1995 Imprint of sub-25 nm vias and trenches in polymers *Applied physics letters* **67** 3114

[17] Chou S Y, Krauss P R and Renstrom P J 1996 25-nanometer resolution *Science272* 85-7

[18] Chou S Y, Krauss P R, Zhang W, Guo L and Zhuang L 1997 Sub-10 nm imprint lithography and applications *Journal of Vacuum Science & Technology B: Microelectronics and Nanometer Structures* **15** 2897-904

[19] Constancias C, Landis S, Manakli S, Martin L, Pain L and Rio D Electron Beam Lithography *Lithography* 101-82

[20] Czaplewski D A, Holt M V and Ocola L E 2013 The range and intensity of backscattered electrons for use in the creation of high fidelity electron beam lithography patterns *Nanotechnology* **24** 305302

[21] Delamarche E, Schmid H, Michel B and Biebuyck H 1997 Stability of molded polydimethylsiloxane microstructures *Advanced Materials* **9** 741-6

[22] Dingemans G, Seguin R, Engelhart P, Sanden M v d and Kessels W 2010 Silicon surface passivation by ultrathin Al2O3 films synthesized by thermal and plasma atomic layer deposition *physica status solidi (RRL)-Rapid Research Letters* **4** 10-2

[23] Duan H, Hu H, Kumar K, Shen Z and Yang J K 2011 Direct and reliable patterning of plasmonic nanostructures with sub-10-nm gaps *ACS nano* **5** 7593-600

[24] Ekinci Y, Solak H H, David C and Sigg H 2006 Bilayer Al wire-grids as broadband and high-performance polarizers *Optics express* **14** 2323-34

[25] Fagan P G, Hammond R B, Roberts K J, Docherty R, Chorlton A P, Jones W and Potts G D 1995 An ab initio approach to crystal structure determination using high-resolution powder diffraction and computational chemistry techniques: Application to 6, 13-dichlorotriphendioxazine *Chemistry of materials* **7** 2322-6

[26] Fergason J L 1983 Liquid crystal display with improved angle of view and response times. Google Patents)

[27] Frounchi M, Mehrabzadeh M and Parvary M 2000 Toughening epoxy resins with solid acrylonitrile–butadiene rubber *Polymer international* **49** 163-9

[28] Gardner E and Hansen D 2003 7.1: An Image Quality Wire-Grid Polarizing Beam Splitter(vol 34): Wiley Online Library) p 62-3

[29] Gates B D and Whitesides G M 2003 Replication of vertical features smaller than 2 nm by soft lithography *Journal of the American Chemical Society* **125** 14986-7

[30] Ge Z and Wu S-T 2008 Nanowire grid polarizer for energy efficient and wide-view liquid crystal displays *Applied Physics Letters* **93** 121104--3

[31] George S M 2009 Atomic layer deposition: an overview *Chemical Reviews* **110** 111-31

[32] Golden J H, DiSalvo F J, Fréchet J M, Silcox J, Thomas M and Elman J 1996 Subnanometer-diameter wires isolated in a polymer matrix by fast polymerization *Science* **273** 782-4

[33] Grigorescu A and Hagen C 2009 Resists for sub-20-nm electron beam lithography with a focus on HSQ: state of the art *Nanotechnology* **20** 292001

[34] Gunning W J and Foschaar J 1983 Improvement in the transmission of iodine-polyvinyl alcohol polarizers *Applied optics* **22** 3229-31

[35] Guo L J 2004 Recent progress in nanoimprint technology and its applications *Journal of Physics D: Applied Physics* **37** R123

[36] Guo L J 2007 Nanoimprint lithography: methods and material requirements *Advanced Materials* **19** 495-513

[37] Hagberg E C, Malkoch M, Ling Y, Hawker C J and Carter K R 2007 Effects of modulus and surface chemistry of thiol-ene photopolymers in nanoimprinting *Nano Letters* **7** 233-7

[38] Han M H and Lyoo W S 2010 Preparation of syndiotacticity-rich high molecular weight poly (vinyl alcohol)/iodine polarizing film with high water resistance *Journal of Applied Polymer Science* **115** 917-22

[39] Hansen D P, Perkins R T and Gardner E 2001 Broad band wire grid polarizing beam splitter for use in the visible wavelength region. Google Patents)

[40] Hollowell A E and Guo L J 2013 Nanowire Grid Polarizers Integrated into Flexible, Gas Permeable, Biocompatible Materials and Contact Lenses *Advanced Optical Materials*

[41] Hsu C-C and Lee Y-C 2010 Fabrication of flexible nano-wired polarizer by contact-transferred and mask embedded lithography and polyurethane acrylate mold: IEEE) p 893-7

[42] Hui C, Jagota A, Lin Y and Kramer E 2002 Constraints on microcontact printing imposed by stamp deformation *Langmuir* **18** 1394-407

[43] Jain A and Bonnecaze R 2013 Fluid management in roll-to-roll nanoimprint lithography *Journal of Applied Physics* **113** 234511

[44] John J, Tang Y, Rothstein J P, Watkins J J and Carter K R 2013 Large-area, continuous roll-to-roll nanoimprinting with PFPE composite molds *Nanotechnology* **24** 505307

[45] Kang M G, Kim M S, Kim J and Guo L J 2008 Organic solar cells using nanoimprinted transparent metal electrodes *Advanced Materials* **20** 4408-13

[46] Khang D-Y, Kang H, Kim T-I and Lee H H 2004 Low-pressure nanoimprint lithography *Nano Letters* **4** 633-7

[47] Kim J K, Cho H S, Jung H-S, Lim K, Kim K-B, Choi D-G, Jeong J-H and Suh K-Y 2012 Effect of surface tension and coefficient of thermal expansion in 30 nm scale nanoimprinting with two flexible polymer molds *Nanotechnology* **23** 235303

[48] Kim S Y, Gwyther J, Manners I, Chaikin P M and Register R A 2013 Metal-Containing Block Copolymer Thin Films Yield Wire Grid Polarizers with High Aspect Ratio *Advanced Materials*

[49] Koch S and Knorr A 2001 Optics in the nano-world *Science* **293** 2217-8

[50] Koo N, Bender M, Plachetka U, Fuchs A, Wahlbrink T, Bolten J and Kurz H 2007 Improved mold fabrication for the definition of high quality nanopatterns by Soft UV-Nanoimprint lithography using diluted PDMS material *Microelectronic Engineering* **84** 904-8

[51] Kumar A and Whitesides G M 1994 Patterned condensation figures as optical diffraction gratings *Science-AAAS-Weekly Paper Edition-including Guide to Scientific Information* **263** 60-1

[52] Lee H, Hong S, Yang K and Choi K 2006 Fabrication of 100 nm metal lines on flexible plastic substrate using ultraviolet curing nanoimprint lithography *Applied physics letters* **88** 143112

[53] Lercel M, Craighead H, Parikh A, Seshadri K and Allara D 1996 Sub-10 nm lithography with self-assembled monolayers *Applied physics letters* **68** 1504-6

[54] Lin P, Pi S, Jiang H and Xia Q 2013 Mold cleaning with polydimethylsiloxane for nanoimprint lithography *Nanotechnology* **24** 325301

[55] Liu X, Deng X, Sciortino P, Buonanno M, Walters F, Varghese R, Bacon J, Chen L, O'Brie N and Wang J J 2006 Large area, 38 nm half-pitch grating fabrication by using atomic spacer lithography from aluminum wire grids *Nano letters* **6** 2723-7

[56] Love J C, Wolfe D B, Chabinyc M L, Paul K E and Whitesides G M 2002 Self-assembled monolayers of alkanethiolates on palladium are good etch resists *Journal of the American Chemical Society* **124** 1576-7

[57] Lowe A, Kwon O-H and Mai Y-W 1996 Fatigue and fracture behaviour of novel rubber modified epoxy resins *Polymer* **37** 565-72

[58] Lucas B D, Kim J S, Chin C and Guo L J 2008 Nanoimprint Lithography Based Approach for the Fabrication of Large-Area, Uniformly-Oriented Plasmonic Arrays *Advanced Materials* **20** 1129-34

[59] Lyoo W S, Yeum J H, Park J M, Kwak J W, Kim J H, Kim S S, Ji B C and Noh S K 2005 Role of molecular weight of atactic poly (vinyl alcohol)(PVA) in the polarizing efficiency of PVA/azo dye complex film with high durability *Journal of applied polymer science* **96** 967-74

[60] Manfrinato V R, Zhang L, Su D, Duan H, Hobbs R G, Stach E A and Berggren K K 2013 Resolution Limits of Electron-Beam Lithography toward the Atomic Scale *Nano letters* **13** 1555-8

[61] Mao A, Schaper C and Karlicek Jr R 2013 Nanopatterning using a simple bi-layer lift-off process for the fabrication of a photonic crystal nanostructure *Nanotechnology* **24** 085302

[62] Mathewson C W 1992 Color display utilizing twisted nematic LCDs and selective polarizers. Google Patents)

[63] McEwan I, Pethrick R A and Shaw S J 1999 Water absorption in a rubber-modified epoxy resin; carboxy terminated butadiene acrylonitrile-amine cured epoxy resin system *Polymer* **40** 4213-22

[64] Miyashita T, Vetter P J, Yamaguchi Y and Uchida T 1995 Wide-viewing-angle display mode for active-matrix LCDs using a bend-alignment liquid-crystal cell *Journal of the Society for Information Display* **3** 29-34

[65] Miyashita T, Yamaguchi Y and Uchida T 1995 Wide-viewing-angle display mode using bend-alignment liquid crystal cell *JAPANESE JOURNAL OF APPLIED PHYSICS PART 2 LETTERS* **34** L 177-L

[66] Moreau W M and Moreau W 1988 *Semiconductor lithography: principles, practices, and materials* vol 233: Plenum Press New York)

[67] Nakayama H, Fukakagawa N, Nishiura Y, Yasuda T, Ito T and Mihayashi K 2006 Development of Low-Retardation TAC Film for Protection Films of LCD's Polarizer *Journal of Photopolymer Science and Technology* **19** 169-73

[68] Odom T W, Love J C, Wolfe D B, Paul K E and Whitesides G M 2002 Improved pattern transfer in soft lithography using composite stamps *Langmuir* **18** 5314-20

[69] Ok J G, Kwak M K, Huard C M, Youn H S and Guo L J 2013 Photo–Roll Lithography (PRL) for Continuous and Scalable Patterning with Application in Flexible Electronics *Advanced Materials* **25** 6554-61

[70] Ok J G, Seok Youn H, Kyu Kwak M, Lee K-T, Jae Shin Y, Jay Guo L, Greenwald A and Liu Y 2012 Continuous and scalable fabrication of flexible metamaterial films via roll-to-

roll nanoimprint process for broadband plasmonic infrared filters *Applied Physics Letters* **101** 223102--4

[71] Pais A, Banerjee A, Klotzkin D and Papautsky I 2008 High-sensitivity, disposable lab-on-a-chip with thin-film organic electronics for fluorescence detection *Lab on a Chip* **8** 794-800

[72] Pang Y-T, Meng G-W, Zhang L-D, Qin Y, Gao X-Y, Zhao A-W and Fang Q 2002 Arrays of ordered Pb nanowires and their optical properties for laminated polarizers *Advanced Functional Materials* **12** 719-22

[73] Park H J, Kang M-G and Guo L J 2009 Large area high density sub-20 nm SiO2 nanostructures fabricated by block copolymer template for nanoimprint lithography *Acs Nano* **3** 2601-8

[74] Pease R 1981 Electron beam lithography *Contemporary Physics* **22** 265-90

[75] Persson C M, Kumpulainen A J and Eriksson J C 2003 Adsorption of n-decyl-β-D-glucopyranoside and n-decyl-β-D-maltopyranoside mixtures at the liquid-vapor interface *Langmuir* **19** 6110-4

[76] Pina-Hernandez C, Fu P-F and Guo L J 2011 Ultrasmall structure fabrication via a facile size modification of nanoimprinted functional silsesquioxane features *ACS nano* **5** 923-31

[77] Pina-Hernandez C, Guo L J and Fu P-F 2010 High-resolution functional epoxysilsesquioxane-based patterning layers for large-area nanoimprinting *ACS nano* **4** 4776-84

[78] Saleh A B, Mohd Ishak Z, Hashim A and Kamil W 2009 Compatibility, mechanical, thermal and morphological properties of epoxy resin modified with carbonyl-terminated butadiene acrylonitrile copolymer liquid rubber *J Phys Sci* **20** 1-12

[79] Scheer H-C, Schulz H, Hoffmann T and Torres S 1998 Problems of the nanoimprinting technique for nanometer scale pattern definition *Journal of Vacuum Science & Technology B: Microelectronics and Nanometer Structures* **16** 3917-21

[80] Schift H 2008 Nanoimprint lithography: an old story in modern times? A review *Journal of Vacuum Science & Technology B: Microelectronics and Nanometer Structures* **26** 458-80

[81] Schmid H and Michel B 2000 Siloxane polymers for high-resolution, high-accuracy soft lithography *Macromolecules* **33** 3042-9

[82] Schubert E F, Wang Y H, Cho A, Tu L W and Zydzik G 1992 Resonant cavity light-emitting diode *Applied physics letters* **60** 921-3

[83] Seo S-m, Kim T-i and Lee H H 2007 Simple fabrication of nanostructure by continuous rigiflex imprinting *Microelectronic engineering* **84** 567-72

[84] Service R 1998 Microelectronics-IBM puts fast chips on a new footing. AMER ASSOC ADVANCEMENT SCIENCE 1200 NEW YORK AVE, NW, WASHINGTON, DC 20005 USA)

[85] Shen Y, Yao L, Li Z, Kou J, Cui Y, Bian J, Yuan C, Ge H, Li W-D and Wu W 2013 Double transfer UV-curing nanoimprint lithography *Nanotechnology* **24** 465304

[86] Shin Y J, Pina-Hernandez C, Wu Y-K, Ok J G and Guo L J 2012 Facile route of flexible wire grid polarizer fabrication by angled-evaporations of aluminum on two sidewalls of an imprinted nanograting *Nanotechnology* **23** 344018

[87] Spurr A R 1969 A low-viscosity epoxy resin embedding medium for electron microscopy *Journal of ultrastructure research* **26** 31-43

[88] Suh D, Choi S J and Lee H H 2005 Rigiflex lithography for nanostructure transfer *Advanced Materials* **17** 1554-60

[89] Suzuki M, Takada A, Yamada T, Hayasaka T, Sasaki K, Takahashi E and Kumagai S 2010 Low-reflective wire-grid polarizers with absorptive interference overlayers: International Society for Optics and Photonics) p 776609--9

[90] Taniguchi J 2013 *Nanoimprint Technology: Nanotransfer for Thermoplastic and Photocurable Polymer*

[91] Tian W-C, Ho Y-H, Chen C-H and Kuo C-Y 2013 Sensing Performance of Precisely Ordered TiO2 Nanowire Gas Sensors Fabricated by Electron-Beam Lithography *Sensors* **13** 865-74

[92] Trimbach D, Feldman K, Spencer N D, Broer D J and Bastiaansen C W 2003 Block copolymer thermoplastic elastomers for microcontact printing *Langmuir* **19** 10957-61

[93] Tsiminis G, Wang Y, Kanibolotsky A L, Inigo A R, Skabara P J, Samuel I D and Turnbull G A 2013 Nanoimprinted Organic Semiconductor Laser Pumped by a Light-Emitting Diode *Advanced Materials*

[94] Van Wijk R J 1995 Fabry-perot with device mirrors including a dielectric coating outside the resonant cavity. Google Patents)

[95] Wang J J, Chen L, Liu X, Sciortino P, Liu F, Walters F and Deng X 2006 30-nm-wide aluminum nanowire grid for ultrahigh contrast and transmittance polarizers made by UV-nanoimprint lithography *Applied physics letters* **89** 141105

[96] Wang J J, Walters F, Liu X, Sciortino P and Deng X 2007 High-performance, large area, deep ultraviolet to infrared polarizers based on 40 nm line/78 nm space nanowire grids *Applied physics letters* **90** 061104--3

[97] Wang J J, Zhang W, Deng X, Deng J, Liu F, Sciortino P and Chen L 2005 High-performance nanowire-grid polarizers *Optics letters* **30** 195-7

[98] Weber T, Käsebier T, Szeghalmi A, Knez M, Kley E-B and Tünnermann A 2011 Iridium wire grid polarizer fabricated using atomic layer deposition *Nanoscale research letters* **6** 1-4

[99] Wu C-L, Sung C-K, Yao P-H and Chen C-H 2013 Sub-15 nm linewidth gratings using roll-to-roll nanoimprinting and plasma trimming to fabricate flexible wire-grid polarizers with low colour shift *Nanotechnology* **24** 265301

[100] Wu S-T 2005 Reflective and transflective liquid crystal display using a wire grid polarizer. Google Patents)

[101] Yabu H, Saito Y, Shimomura M and Matsuo Y 2013 Thermal nanoimprint lithography of polymer films on non-adhesive substrates by using mussel-inspired adhesive polymer layers *Journal of Materials Chemistry C* **1** 1558-61

[102] Yeh P 1978 A new optical model for wire grid polarizers *Optics Communications* **26** 289-92